Check for updates

The role of humic-type ligands in the bioavailability and stabilization of dissolved iron in the Western Tropical South Pacific Ocean

Gabriel Dulaquais[1]*, Pierre Fourrier[1], Cécile Guieu[2],
Léo Mahieu[3], Ricardo Riso[1], Pascal Salaun[3], Chloé Tilliette[2]
and Hannah Whitby[3]

[1]Laboratoire des Sciences de l'Environnement Marin Centre nationale pour la recherche scientifiques
(CNRS) UMR 6539, Institut Universitaire Européen de la Mer, Université de Bretagne Occidentale,
Plouzané, France, [2]Sorbonne Université, Centre nationale pour la recherche scientifiques (CNRS),
Laboratoire d'Océanographie de Villefranche (LOV), Villefranche-sur-Mer, France, [3]Department of
Earth, Ocean and Ecological Sciences, School of Environmental Sciences, University of
Liverpool, United Kingdom

The high N_2 fixation rate observed in the Lau Basin of the western tropical South Pacific Ocean (WTSP) is fueled by iron (Fe) released from shallow hydrothermal systems. Understanding Fe bioavailability is crucial but the controls on the stability and bioavailability of hydrothermal Fe inputs are still poorly understood. Here, we provide new data on the spatial and vertical distribution of the soluble ubiquitous humic-like ligands (L_{FeHS}) and their associated dissolved Fe (DFe) in the WTSP, including in samples near hydrothermal vents. Our data show that L_{FeHS} are heterogenous ligands with binding sites of both strong and intermediate strengths. These ligands are primarily produced in surface waters and partially mineralized in mesopelagic waters. A substantial fraction of DFe was complexed by L_{FeHS} (mean ~30%). The DFe complexed by L_{FeHS} is likely bioavailable to phytoplankton and L_{FeHS} stabilized Fe released by the mineralization of sinking biomass. However, unsaturation of L_{FeHS} by Fe suggest that part of DFe is not available for complexation with L_{FeHS}. Possible reasons are competition between DFe and other metals, such as dissolved copper, or the inability of L_{FeHS} to access colloidal DFe. The study of two volcanic sites indicates that L_{FeHS} were not produced in these hydrothermal systems. At the active site (DFe ~50 nmol L^{-1}), L_{FeHS} can only partially solubilize the hydrothermal DFe released in this area (1~5.5% of the total DFe). We performed controlled laboratory experiments which show that the observed low solubilization yield result from the inability of L_{FeHS} to solubilize aged Fe oxyhydroxides (FeOx - a kinetically mediated process) and to form stable complexes with Fe(II) species. Our study provides new understanding of the role of L_{FeHS} on the bioavailability and stabilization of hydrothermal DFe.

KEYWORDS

iron, organic complexation, humic substances, hydrothermal vents, Pacific Ocean

1 Introduction

Iron (Fe) bioavailability is crucial for marine life and across a large part of the ocean, primary producers are Fe limited or co-limited (Moore et al., 2013). In seawater, dissolved Fe (DFe) geochemistry is governed by complex redox chemistry limiting the solubility of inorganic DFe at subnanomolar levels (e.g., Sung and Morgan, 1980; Millero et al., 1987; Martin and Fitzwater, 1988; Martin and Gordon, 1988; Martin et al., 1989; Martin et al., 1991; Byrne et al., 2000; Rose and Waite, 2003a; Santana-Casiano et al., 2005; Croot and Heller, 2012). Large-scale measurements of oceanic DFe concentrations conducted in the context of the GEOTRACES program (Schlitzer et al., 2018) evidenced that DFe can be found at higher concentrations than the subnanomolar solubility limit predicted by Liu and Millero (2002). These observations indicate that other processes are involved in controlling Fe solubility in the dissolved phase: organic complexation and colloidal precipitation. Colloidal DFe (0.02 µm< cFe< 0.450 µM) represents a significant fraction (up to > 50%) of oceanic total DFe and has a pivotal role in DFe dynamics (Nishioka et al., 2001; Wu et al., 2001; Boye et al., 2010; Fitzsimmons and Boyle, 2014; Kunde et al., 2019). Chelation with organic ligands enhances Fe solubility and almost all DFe is thought to be complexed by natural ligands in seawater (Gledhill and van den Berg, 1994; Rue and Bruland, 1995; van den Berg, 1995; Wu and Luther, 1995) including in the colloidal phase (Boye et al., 2010; Fitzsimmons et al., 2015). The sources, distributions, chemical functions and reactivity of these ligands need to be assessed to improve our understanding of DFe biogeochemistry (Macrellis et al., 2001; Hunter and Boyd, 2007; Benner, 2011; Gledhill and Buck, 2012; Bundy et al., 2015; Hassler et al., 2017). Organic iron-binding ligands (L_{Fe}) are themselves part of the dissolved organic carbon (DOC) pool, the largest organic carbon pool in the ocean (Guo et al., 1995), but the wide variety of ligand types is a barrier for detailed characterization of these organic compounds. Discrimination of ligand classes using cathodic stripping voltammetry with competing ligand exchange (CLE-CSV) is the most commonly used method to quantify L_{Fe} (Gledhill and Buck, 2012). CLE-CSV methods permit an operational classification of ligands depending on their binding strength. According to the Gledhill and Buck (2012) classification, there are the strong (L_1, log $K_{Fe'L1} > 12$), the intermediate (L_2, $11 \leq$ log $K_{Fe'L2} \leq 12$) and the weak classes (L_3, log $K_{Fe'L3<} 11$). Another weaker class (L_4 log $K_{Fe'L3<} 10$) can even be introduced for L_{Fe} of very low strength. Nevertheless, CLE-CSV have methodological caveats (Gerringa et al., 2021) and the presence of non-labile DFe species for complexation with the competing ligand can lead to over- and underestimations of L_{Fe}. Futhermore, relying solely on Log $K_{Fe'L}$ for the classification of L_{Fe} may yield inaccurate results due to the heterogeneity of ligand binding sites. It may be more relevant to consider reactivity coefficients ($\alpha FeL(Fe') = $ log $K_{Fe'L} * LFe'$), as suggested by Gledhill and Gerringa (2017). Reactivity coefficients express the probability that any added metal will be complexed by the ambient free ligands. Advances in mass spectrometry open perspectives for the study of siderophores, a class of strong ligands (Gledhill, 2001; McCormack et al., 2003; Mawji et al., 2008; Boiteau and Repeta, 2015). Environmental studies have shown that siderophore compounds are present at picomolar levels in seawater (Bundy et al., 2018; Hawco et al., 2021), far lower than nanomolar ambient L_{Fe} concentrations recorded in seawater (Buck et al., 2018). Thereby, efforts must be conducted to study other ligand types such as polyphenol compounds, extracellular polymeric substances (EPS) and humic substances (HS). In this work we will focus on the role of HS in the stabilization and bioavailability of DFe.

Maillard (1912) described the chemistry of HS for the first time, and this terminology encompasses several definitions, depending on the type of measurement applied to the particulate or dissolved fraction (Davies and Ghabbour, 2003; Riso et al., 2021). HS can be operationally separated into their soluble (fulvic acids) and insoluble (humic acids) parts under acidic conditions (MacCarthy et al., 1979; Thurman and Malcolm, 1981; De Paolis and Kukkonen, 1997). Marine HS are believed to originate from the decomposition of (macro)biomolecules (derived from phytoplankton) microbially-degraded in the ocean interior (Hedges et al., 1992; Tranvik, 1993; Hertkorn et al., 2006). The importance of HS in the stabilization of trace metals in the dissolved phase is known since the early 80's (Boggs et al., 1985) but the difficulties to isolate HS from seawater prevented the study of these compounds and their interactions with Fe for decades.

Recent studies demonstrate the ubiquity of HS in the ocean accounting for more than half of the DOC oceanic concentrations (Zigah et al., 2017; Fourrier et al., 2022). Among the different compounds contributing to HS, some are "electroactive" (called eHS) and able to complex trace elements. The electroactivity is a property of HS measurable by electrochemical methods (Whitby and van den Berg, 2015; Dulaquais et al., 2018a; Sukekava et al., 2018). Electroactivity of HS is representative of the density of the functional groups involved in metal complexation. For Fe and other metals such as copper (Cu), the latter seem to be oxygen-containing functional groups such as carboxyl and phenol moieties (Blazevic et al., 2016). Electroactivity can be converted into concentration of iron-binding ligand of humic nature (L_{FeHS}) providing a quantification of this ligand class. Field measurements show that electroactivity strongly decreases from fresh to marine waters (Riso et al., 2021) and from subsurface to deep waters in the ocean (Dulaquais et al., 2018a; Fourrier et al., 2022). *In situ* experiments conducted by Whitby et al. (2020a) showed that microbial degradation results in a release of eHS, but at high POC degradation rate, there was also concurrent eHS removal. As a result, the impacts of biogeochemical processes (e.g. mineralization, photobleaching) on this property (e.g. electroactivity) remain unclear. In regard to CLE-CSV data, L_{FeHS} are mainly assigned to the intermediate class of ligand (e.g. L_2; Laglera and van den Berg, 2009; Gledhill and Buck, 2012) but this complex mixture possibly includes components of other classes (Perdue and Lytle, 1983; Laglera et al., 2019; Gledhill et al., 2022). Field observations (Buck et al., 2018) and numerical simulations (Misumi et al., 2013) suggest that L_2 type ligands regulate the DFe distribution as well as its residence time in the deep ocean (Hunter and Boyd, 2007). Interactions between Fe and L_{FeHS} were previously investigated by measuring both parameters independently (Laglera and van den Berg, 2009; Batchelli et al., 2010; Bundy et al., 2014; Bundy et al.,

2015; Krachler et al., 2015; Slagter et al., 2017; Dulaquais et al., 2018a) raising ever more questions on the links between the biogeochemistry of both parameters. Considering the occurrence of L_{FeHS} throughout the water column (Dulaquais et al., 2018a; Laglera et al., 2019; Whitby et al., 2020b; Fourrier et al., 2022), the role of L_{FeHS} in the Fe marine biogeochemistry needs to be further considered.

Thanks to the optimization of electrochemical methods, there is now the possibility to quantify the effective amount of Fe complexed by L_{FeHS} (DFe-HS) in a natural sample (Sukekava et al., 2018). The first application of this methodology on samples from the Arctic Ocean evidenced that DFe-HS represents ~80% of total DFe in this basin impacted by riverine inputs (Laglera et al., 2019). This has large implications for our understanding of DFe export from the surface Arctic to the deep Atlantic and encourages the scientific community to extend these kinds of measurements to other oceanic basins submitted to different forcing. Indeed, to confirm the importance of L_{FeHS} in Fe biogeochemistry, we need new data from contrasting environments such as deep environments where data are still scarce (Whitby et al., 2020b). In particular, studies of hydrothermal systems – that provide a large amount of DFe to the deep ocean (e.g. Tagliabue et al., 2010; Resing et al., 2015) – have so far not established a link between L_{FeHS} and DFe. In these extreme environments with low pH and low O_2, a significant large fraction of DFe can can exist in its reduced form as Fe(II) (González-Santana et al., 2021; González-Santana et al., 2023). It has been observed that humic type DOM catalyse the oxidation of Fe(II) (Santana-Casiano et al., 2022) and that some polyphenols reduce Fe(III) into Fe(II) (González et al., 2019; Pérez-Almeida et al., 2022). However, the capacity of L_{FeHS} to form stable complexes with Fe(II) in marine waters remains poorly explored.

In this context, we explored the spatial distributions of L_{FeHS} and DFe-HS in the oligotrophic waters of the Western Tropical South Pacific Ocean (WTSP). With the aim to shed light on the role of L_{FeHS} in the stabilization of hydrothermal DFe, samples were collected along a 6100 km transect partly impacted by shallow hydrothermal vents (TONGA GEOTRACES GPr14 expedition; https://doi.org/10.17600/18000884). As Fe oxyhydroxides (FeOx) can be massively released by hydrothermal systems and can persist under colloidal form in the distal plume (Fitzsimmons et al., 2017; Lough et al., 2019), we conducted complementary kinetic experiments to shed light on the capacity of L_{FeHS} to solubilize FeOx in seawater.

2 Materials and methods

2.1 Sampling strategy and collection of samples

Samples were collected during the TONGA GEOTRACES GPpr14 expedition onboard the R/V *L'Atalante* in November 2019 (20°S – 24°S; -166°W – 165°W). This 6100 km-long transect encountered three biogeochemical zones (Figure 1). As described in Tilliette et al. (2022), two types of stations were sampled during the expedition: eight short-duration stations (SD 2, 3, 4, 6, 7, 8, 11, and
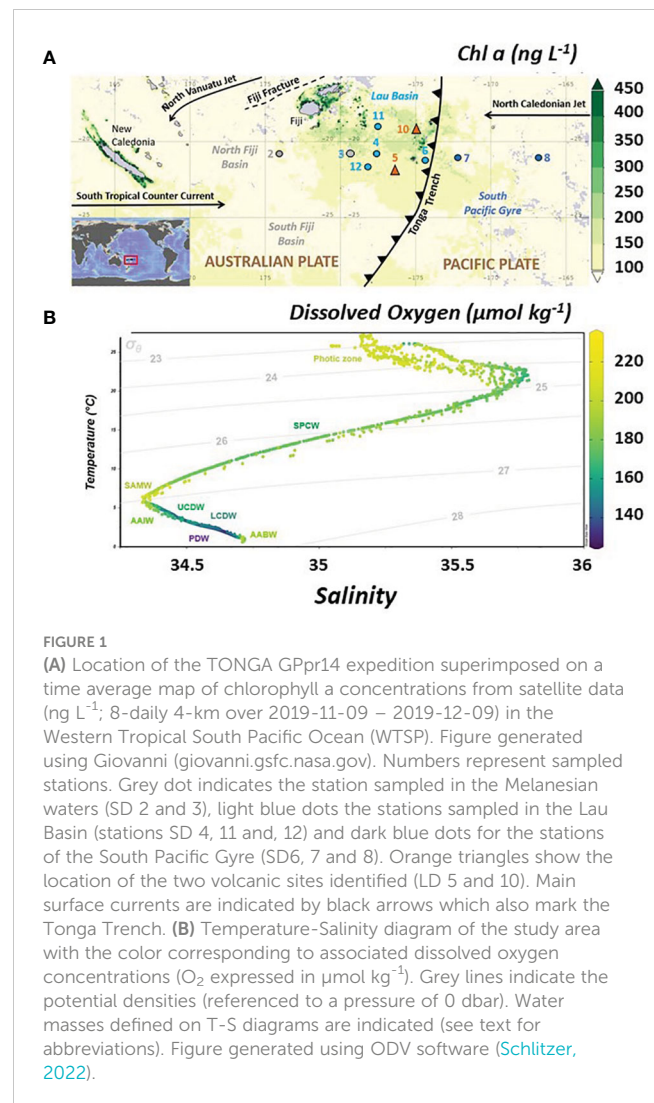

FIGURE 1
(A) Location of the TONGA GPpr14 expedition superimposed on a time average map of chlorophyll a concentrations from satellite data (ng L^{-1}; 8-daily 4-km over 2019-11-09 – 2019-12-09) in the Western Tropical South Pacific Ocean (WTSP). Figure generated using Giovanni (giovanni.gsfc.nasa.gov). Numbers represent sampled stations. Grey dot indicates the station sampled in the Melanesian waters (SD 2 and 3), light blue dots the stations sampled in the Lau Basin (stations SD 4, 11 and, 12) and dark blue dots for the stations of the South Pacific Gyre (SD6, 7 and 8). Orange triangles show the location of the two volcanic sites identified (LD 5 and 10). Main surface currents are indicated by black arrows which also mark the Tonga Trench. **(B)** Temperature-Salinity diagram of the study area with the color corresponding to associated dissolved oxygen concentrations (O$_2$ expressed in µmol kg^{-1}). Grey lines indicate the potential densities (referenced to a pressure of 0 dbar). Water masses defined on T–S diagrams are indicated (see text for abbreviations). Figure generated using ODV software (Schlitzer, 2022).

12) and two long-duration stations (LD 5 and 10), the latter two dedicated to the study of the dispersion of hydrothermal fluids. These two LD stations included 5 (for LD 5) and 4 (for LD 10) subcasts, named from T5 to T1, with T5 being the closest to the hydrothermal source. Hydrothermal sources were detected from the acoustic anomalies (Bonnet et al., 2023) using a multibeam echosounder (hull-mounted EM-710 echosounder of R/V *L'Atalante*), operating at a frequency of 70–100 kHz for depths shallower than 1000 m. As described in Tilliette et al. (2022), the T5 substations were positioned where the highest acoustic anomalies were recorded at 200 and 300 m for LD 5 and 10, respectively. At both LD 5 and 10, the other substations (T1, T2, T3, T4 for LD 5 and T1, T2, T3 for LD 10) were positioned west of "T5" according to the main surface current direction in order to investigate the longitudinal impact of hydrothermal fluids released from T5 (see Supporting informations in Tilliette et al., 2022 for further details of positions). At LD 10, an additional substation called "Proxnov" (i.e., Metis Shoal; 19.18°S, 174.87°W) located further north of this site (15 km from LD 10-T5) was sampled to capture the eruption of the Late'iki submarine volcano that occurred one month prior to the expedition (Plank et al., 2020).

Sampling was operated using a trace metal clean polyurethane powder-coated aluminum frame rosette (TMR) equipped with twenty-four 12 L Teflon-lined GO-FLO bottles (General Oceanics) and attached to a Kevlar® wire. Potential temperature (θ), salinity (S) and dissolved oxygen (O_2) were retrieved from the conductivity–temperature–depth (CTD) sensors (SBE9+) deployed on the TMR. The cleaning protocols of all the sampling equipment followed the guidelines of the GEOTRACES Cookbook (http://www.geotraces.org). After recovery, the TMR was directly transferred into a clean container equipped with a class 100 laminar flow hood. Samples were then taken from the filtrate of particulate samples (collected on acid-cleaned polyethersulfone filters, 0.45 μm supor). For L_{FeHS}, L_{Fe} and DOC, the filtrate was collected into acid-cleaned and sample-rinsed high density polyethylene (HDPE) 125 mL bottles. Immediately after collection, samples were double-bagged and stored at -20°C until analysis in a shore-based laboratory. For DFe, the filtrate was collected into acid-cleaned and sample-rinsed 60 mL HDPE Nalgene bottles, acidified to pH ~1.7 with Ultrapure HCl (0.2% v/v, Supelco®) within 24 h of collection and stored double-bagged pending analysis at Laboratoire d'Océanographie de Villefranche (full protocol and data in Tilliette et al., 2022).

2.2 Reagents

All aqueous solutions and cleaning procedures used ultrapure water (resistivity > 18.2 MΩ.cm^{-1}, MilliQ Element, Millipore®). An acidic solution (hydrochloric acid, HCl, 0.01 M, Suprapur®, >99%) of 1.24 μmol L^{-1} Fe (III) was prepared daily from a stock solution (1 g L^{-1}, VWR, Prolabo, France). The borate buffer (H_3BO_3, 1M, Suprapur®, Merck, Germany, 99.8%) was prepared in 0.4 M ammonium solution (NH_4OH, Ultrapure normatom, VWR Chemical, USA, 20-22%). The potassium bromate solution ($KBrO_3$, 0.3 M, VWR Chemical, USA, ≥ 99.8%) was prepared in ultrapure water. *Suwannee River Fulvic Acids* (SRFA, 1S101F) were purchased at the International Humic Substances Society (IHSS). The SRFA standard stock solution (22.86 mg SFRA L^{-1}) was prepared in ultrapure water and saturated with iron according to its iron binding capacity in seawater determined by Sukekava et al. (2018). Saturated SRFA solution was equilibrated overnight before its use. Exact concentration of the SRFA stock solution was determined by size exclusion chromatography analysis (Dulaquais et al., 2018b). A 10^{-3} M Gallic Acid (GA) stock solution (Sigma-Aldrich) was prepared in HPLC grade methanol, as described in González et al. (2019). The second GA stock solution (10^{-6} M) was prepared in ultrapure water. The second stock solution of GA was divided into two portions, with one portion saturated with Fe (final concentration of 5 10^{-6} M Fe). Following an overnight equilibration, the Fe-saturated solution was filtered through a 0.02 μm filter to remove any excess iron that precipitated as FeOx.

FeOx dissolution experiments. Artificial seawater (Salinity = 35; pH = 8.2 ± 0.05) was prepared by dissolving sodium chloride (NaCl, 6.563 g, ChemaLab NV, Belgium, 99.8%), potassium chloride (KCl, 0.185 g, Merck, Germany, 99.999%), calcium chloride (CaCl$_2$,

0.245 g, Prolabo, France, > 99.5%), magnesium chloride (MgCl$_2$, 1.520 g, Merck, Germany, 99-101%), magnesium sulfate (MgSO$_4$, 1.006 g, Sigma-Aldrich, USA, ≥99%) and sodium bicarbonate (NaHCO$_3$, 0.057 g, ChemaLab NV, Belgium, >99.7%) in ultrapure water (250 mL). Artificial seawater was then UV irradiated for 2 hours in order to remove all traces of organic compounds. The UV system consisted of a 125-W mercury vapor lamp with 4 30-mL PTFE-capped quartz tubes (http://pcwww.liv.ac.uk/~sn35/Site/UV_digestion_apparatus.html).

2.3 Analysis of iron-binding ligands of humic type and of dissolved iron-humic concentrations

The determination of L_{FeHS} was performed on 213 samples from the eight SD and on the two LD stations, including all LD substations, with half the depth resolution. L_{FeHS} is based on the determination of electroactive humic substances (eHS). Analyses were operated by cathodic stripping voltammetry (CSV) using a polarographic Methrom 663VA stand connected to a potentiostat/galvanostat (μautolab 2, Methrom®) and to an interface (IME 663, Methrom®). Data acquisition was done using the NOVA software (version 10.1). The method used in this study was initially developed by Laglera et al. (2007) and adapted by Sukekava et al. (2018). The method is based on the adsorption at pH 8 of a Fe-humic complex at the surface of a mercury drop electrode under a potential fixed at -0.1 V (vs Ag/AgCl) and its reduction during linear stripping of potentials (0.1 to 0.8 V). In the presence of 30 mmol L^{-1} bromate, the reduction of the Fe-humic complex provides a quantitative peak at -0.5 V (vs Ag/AgCl) with an intensity proportional to the concentration. In this study, the samples were defrosted at 4°C and 100 mL were poured in a 250 mL Teflon® bottle. pH was then set to 8.00 ± 0.05 by addition of a borate buffer (final concentration = 10 mM) and adjusted by small additions of an ammonia solution. A first aliquot of the sample was poured into Teflon® vials (Savillex®) in order to detect the natural iron-humic complex (Sukekava et al., 2018). The sample (remaining in the 250 mL Teflon® bottle) was then spiked with 10 nmol L^{-1} of Fe to saturate all eHS (and others L_{Fe}) in the initial sample. After equilibration (1h), 3 others aliquots (15 mL) of the sample were placed into 3 Teflon® vials (Savillex®). Among them, two were spiked with a SRFA standard (1S101F; standard additions of 50 and 100 μg L^{-1}, respectively) and left for overnight equilibration. After equilibration, the 4 aliquots of samples (1 without Fe, 1 with Fe and 2 with Fe and SRFA additions)were successively placed into a Teflon® voltammetric cell and analyzed by linear sweep voltammetry as described above after 180 s of nitrogen (N_2) purge (Alphagaz®, Air liquide) and a 90 s deposition step at –0.1V. The absence of quantitative signals in MilliQ water ensured no contamination along the entire analytical process. Peak heights were extracted to determine the electroactive humic concentrations (determined in μg eq-SRFA L^{-1}). Errors of these measurements were determined using a least-squares fit function. We converted eHS

concentrations into L_{FeHS}, as described by Sukekava et al. (2018), using the binding capacity of the model humic-type ligand SRFA used (1S101F) for DFe in seawater (14.6 ± 0.7 nmol Fe mgSRFA^{-1}; Sukekava et al., 2018). Similar conversions have been previously used in the recent literature (Dulaquais et al., 2018a; Laglera et al., 2019; Whitby et al., 2020b; Fourrier et al., 2022). The limit of detection (LOD) for 90 s of deposition time was calculated as three times the mean standard deviation of all samples analyzed (n = 213). LOD was estimated at 0.11 nmol eq-Fe L^{-1}. After data treatment, 12 samples were below the calculated LOD. These samples were mostly within the 200-1000 m depth range where L_{FeHS} displays their minimal concentrations (Figure 2). They were discarded from the dataset resulting in 201 datapoints for L_{FeHS}.

Voltammetric peaks of the first (i0, pH adjusted sample) and second (i1, pH adjusted and Fe saturated) aliquots permits the determination of the initial amount of DFe bound to humic-type ligands in the sample. This was determined according to equation (1), first introduced by Sukekava et al., 2018.

$$[DFe - HS]_{sample} = i0/i1 * L_{FeHs\ sample} \qquad (1)$$

As no DFe-HS blank signal can be determined (several samples with no i0 signal), the LOD was defined as three times the standard deviation of the lowest DFe-HS concentration ([DFe-HS]) measured (0.01 ± 0.01 nmol eqFe L^{-1}) and was estimated to be 0.03 nmol eq-Fe L^{-1}. After data treatment, 14 samples had a [DFe-HS] below the calculated LOD; they were removed from the dataset resulting in 187 datapoints for DFe-HS.

Further discussion about the the relevance of the methodology to determine L_{FeHS} can be found in the Supplementary Information.

2.4 Dissolution of iron oxyhydroxide by L_{FeHS}

Experimental dissolutions of FeOx by humic-type ligands were carried out as a function of time and age of FeOx. 250 mL of UV irradiated artificial seawater was spiked with 100 nmol L^{-1} Fe. In the absence of organic ligands, the limit of solubility of DFe is subnanomolar (Liu and Millero, 2002), thereby DFe would

rapidly form Fe oxyhydroxides (Rose and Waite, 2003b). Fe-spiked artificial seawater was then placed on an agitation table (320 rpm, IKA$^®$KS basic) all along the duration of the experiment. After intense shaking by hand (10 s), a single aliquot (1.5 mL) of Fe-spiked artificial seawater was sampled at 1 min, 1 h, 6 h and every day over the course of one week and then at two weeks after FeOx initial formation. Aliquots of the FeOx solution were directly transferred to 13.5 mL of a SRFA solution (buffered pH = 8.00 ± 0.05, final concentration 0.5 mg-SRFA L^{-1} in UV irradiated artificial seawater) in a Teflon voltammetric cell. After an initial N$_2$ purge of 180 s, the dissolution kinetic of FeOx by SRFA was followed by CSV during 30 cycles using the same voltametric conditions as described in section 2.3 with N$_2$ purge and deposition times set at 15 s and 90 s, respectively. The experiment was run in duplicate and was reproducible ensuring reproducibility of the experiment. Measurement of pH at the end of the experiment indicated no significant variation, confirming the stability of the pH within the voltammetric cell throughout the duration of the experiment (1 hour).

2.5 Competition between natural humic-type ligands with gallic acid for iron complexation

The Fe-binding strength of natural humic-type ligands was determined by ligand competition experiments between natural samples and gallic acid (GA). Experiments were conducted on (1) surface seawater collected at 25 m at station 6 (outside the Lau Basin). The experiment (see design of experiment in supplementary information) is based on the measurement of the FeHS voltammetric signal in the same sample that has undergone different additions of DFe and/or GA. The binding properties of GA for Fe (III) used are those described in González et al. (2019) (L_{FeGA} = 2.75 nmol Fe nmol GA^{-1}; LogK$_{FeGa}$ = 9.1).

The competition for Fe' is based on the equilibrium between DFe and L_{FeHS} (equation 2) and between DFe and GA (equation 3).

$$K_{FeHS} = \frac{[DFeHS]}{[LFeHS']*[Fe']} \qquad (2)$$
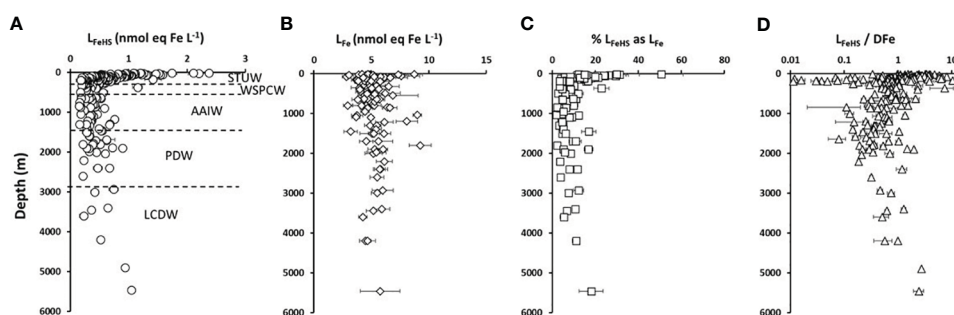
FIGURE 2
Vertical distribution with depth of **(A)** humic type ligands (circles, L_{FeHS}, n = 203), **(B)** Iron binding ligands (diamonds, LFe, n = 103) and **(C)** % L_{Fe} of humic nature (squares, n = 103) measured along the water column during the TONGA expedition. **(D)** L_{FeHS} over DFe ratio (triangles, L_{FeHS}/DFen = 203). Water masses identified by multiparametric optimal analysis and their associated depths are indicated in **(A)** see text for water masses acronyms.

$$K_{FeGA} = \frac{[DFeGA]}{[GA']*[Fe']} \qquad (3)$$

$$DFe = DFeHS + DFeGA + Fe' \qquad (4)$$

With K_{FeHS} and K_{FeGA}, the conditional stability constants of natural humic-type ligands and of gallic acid for DFe, respectively, [DFeHS]; the concentration of Fe bound to natural humic type ligands calculated using the binding capacity of SFRA, $[L_{FeHS}]'$; the unsaturated humic-type ligand concentration; $[Fe]'$, the inorganic Fe species; [DFeGA], the concentration of Fe bound to gallic acid and $[GA]'$, the concentration of unsaturated Gallic acid ligands.

When the two ligands are in competition, the conditional stability constant of the natural humic-type ligands can be calculated according to equation 4.

$$K_{FeHS} = \frac{[DFeHS]*[GA']}{[DFeGA]*[LFeHS']}*K_{FeGA} \qquad (5)$$

The FeHS voltametric signal increasing linearly with Fe, the Fe concentration complexed by humic-type ligands can be determined as the ratio between the FeHS signal for a given experimental condition and the FeHS signal of the samples when saturated with dFe (L_{FeHS}) multiplied by the binding capacity of the sample (see equation 1). Assuming that eHS only complex with Fe, the free humic-type ligands can be then determined using equation 6.

$$[L_{FeHS}'] = [DFeHS] - L_{FeHS\ sample} \qquad (6)$$

Assuming that Fe" is negligible over DFe, the concentration of FeGA complex can be estimated using equation 7.

$$[DFeGA] \sim DFe - [DFeHS] \qquad (7)$$

Assuming that GA only complex Fe, when GA is added with a known concentration in a sample, $[GA']$ can be calculated from the total concentration of added GA ($L_{FeGA\ sample}$) according to equation 8.

$$[GA'] = L_{FeGA\ sample} - [DFeGA] \qquad (8)$$

2.6 Dissolved iron analysis

DFe concentrations were measured by flow injection and chemiluminescence detection (FIA-CL) in a clean room at the Laboratoire d'Océanographie de Villefranche. The method, data and analytical performance are fully presented in Tilliette et al. (2022). The DFe-rich samples were diluted in DFe-depleted seawater collected at SD 8. The final concentration of those diluted samples did not exceed 5 nmol L^{-1} and a 0-5 nmol L^{-1} calibration curve was used in that case. Each sample was analyzed in triplicate. The mean analytical blank was 21 ± 22 pM and the detection limit was 16 ± 7 pM. Method accuracy was evaluated daily by analyzing the GEOTRACES Surface (GS) seawater (DFe = 0.510

± 0.046 nmol L^{-1}; n = 24) which compares well with community consensus concentrations of 0.546 ± 0.046 nmol L^{-1}.

2.7 Analysis of dissolved organic carbon concentrations

Dissolved organic carbon concentrations were determined by size exclusion chromatography with multi-detectors according to the methodology described in Fourrier et al. (2022). Accuracy of measurements were checked by analyzing deep sea reference samples (DSR, Hansell lab, Florida) each set of ten samples.

2.8 Analysis of iron-binding ligands

Iron-binding ligands (L_{Fe}) were determined for 103 samples by Mahieu et al. (this issue) using competitive ligand exchange with adsorptive cathodic stripping voltametry (CLE-ACSV). The theory of the CLE-ACSV is presented with great detail in the literature (e.g. Gledhill and van den Berg, 1994; Rue and Bruland, 1995; Abualhaija and van den Berg, 2014; Gerringa et al., 2014; Pižeta et al., 2015). For acquisition of L_{Fe} data, samples were buffered at pH of 8.2 (1 M boric acid, in 0.35 M ammonia) and separated in 16 aliquots. Then natural ligands were left to equilibrate with DFe levels of 0, 0, 0.75, 1.5, 2.25, 3, 3.5, 4, 4.5, 5, 6, 7, 8, 10, 12 and 15 nmol.L^{-1} in the 16 aliquots. The artificial ligand added was salycilaldoxime (SA; 98%; Acros Organics™) at final concentration of 25 μmol.L^{-1} resulting to a detection window (D) of 79 (Buck et al., 2007). Analyses were operated on a 663 VA stand (Metrohm™) under a laminar flow hood (class-100), supplied with nitrogen and equipped with a mercury drop electrode (MDE, Metrohm™), a glassy carbon counter electrode and a silver/silver chloride reference electrode (3M KCl) in a Teflon voltametric cell. During the voltammetric measurement, the sample was kept oxygenated by a constant air-flow at the surface and the nitrogen gas flow from the 663 VA stand above the sample was stopped. Detailed procedure can be found in Mahieu et al. (this issue).

2.9 Statistics

A Shapiro-Wilk test was used to verify that the data follows a normal distribution, and the homogeneity of variances was assessed by conducting a Levene's test. Significance in linear regression analysis was determined using the Pearson test. In cases of normally distributed datasets, the significance of differences between data was examined using t-tests. For non-normally distributed datasets, a non-parametric Wilcoxon-Mann Whitney test was utilized to evaluate the significance of differences. A probability value (p) less than 0.05 was considered statistically significant for all analyses.

3 Results

3.1 Hydrography and hydrothermal context

Three distinct basins were crossed and sampled during the TONGA expedition (Figure 1A). The Melanesian waters (grey dots, SD2 and 3), the Lau Basin (average depth shallower than 2000 m) (Figure 1A, clear blue dots and orange triangles, SD4, 11 and 12, LD5 and 10) and the South Pacific Gyre, east of the Tonga Kermadec Arc (dark blue dots, SD 6, 7 and 8). In the Lau Basin, two shallow volcanic systems hosting hydrothermal sites were studied (Figure 1, orange triangles), referred to LD 5 and LD 10. The hydrothermal system at LD 5 was active and marked by high DFe concentrations, up to 50 nmol L^{-1}, close to the vent (Tilliette et al., 2022). In contrast, the activity at LD 10 had likely been considerably slowed down at time of sampling, possibly due to the eruption of the nearby *Late'iki* volcano (Plank et al., 2020). Nevertheless, LD 10 water composition was probably impacted, at least for DFe, by the volcanic activity of the shallow hydrothermal site in the upper 300 m and of *Metis* at depths deeper than 1000 m (Tilliette et al., 2022; Tilliette et al., sub.).

Low surface chlorophyll *a* concentrations (< 0.2 mg m^{-3} derived from satellite data, MODIS-Aqua MODISA simulations, Figure 1A) and extremely low nutrient concentrations (NO$_3^-$ and PO$_4^{3-}$< 50nmol L^{-1}, https://www.seanoe.org/data/00770/88169/) reflect the ultra-oligotrophy of the North Fiji basin and South Pacific Gyre at the time of sampling. The Lau Basin was marked by higher surface chlorophyll *a* concentrations than the subtropical gyre (Figure 1) indicating that primary production was enhanced in this area. Bonnet et al. (accepted) have shown the causal link between this increased productivity due to diazotrophic organisms whose iron needs are very important and the shallow hydrothermal sources that bring the necessary iron to the surface.

The water masses along the transect area were extensively studied in Tilliette et al. (2022) using hydrographic properties collected during the TONGA expedition as well as a multiparametric optimal analysis (OMP). The main thermocline (200-700 m) includes the Surface Tropical Underwater (STUW) and the Western South Pacific Central Water (WSPCW). The STUW originates from the subduction of high salinity waters from the equatorial part of the subtropical gyre and is associated with a shallow salinity maximum. Created by subduction and diapycnal mixing, the WSPCW exhibits a linear relationship between temperature and salinity over a wide range up to the intermediate layer. The intermediate layer (700-1300 m) was composed solely of AAIW, a low salinity water mass originating from the sea surface at sub-Antarctic latitudes and characterized by a minimum salinity reached at 700 m. AAIW circulates around the subtropical gyre from the south-east Pacific, spreading north-westwards as tongues of low-salinity, high-oxygen water, and enters the tropics in the western Pacific. The deep layer (> 1300 m) contains the Pacific Deep Water (PDW) and the Lower Circumpolar Deep Water (LCDW). The PDW originates from the equatorial Pacific and flows southwards. It is formed in the interior of the Pacific from upwelling of Antarctic Bottom Water (AABW).

PDW is characterized by low oxygen content and well-mixed temperature and salinity. LCDW originates from the Southern Ocean and overlaps the depth and density ranges of PDW. However, it differs from the PDW by a maximum of salinity and oxygen. The OMP results revealed a uniform distribution of water masses along the transect, except the two deep water masses, PDW and LCDW, for which differences could be observed in their distribution west and east of the Tonga Arc. STUW is mainly present at depths between 150 and 300 m, followed by WSPCW which is predominantly present between 300 and 500 m. AAIW dominated the entire transect over a wide depth range from 500 to 1300 m. A major contribution from PDW was found west of the Tonga Arc from 1300 m to the seafloor, while PDW only occupied depths between 1300 and 3000 m east of the arc. Below 3000 m LCDW dominated (Tilliette et al., 2022). It is worth noting that Upper Circumpolar Deep Water (UCDW) and AABW were detected according to their salinity and Temperature (Figure 1) however the OMP operated by Tilliette et al. (2022) revealed a zero contribution from these water masses along the transect.

3.2 Vertical distribution of iron-binding ligands of humic-type

Along the TONGA section, concentrations of L$_{FeHS}$ ranged from 0.15 ± 0.05 to 2.38 ± 0.05 nmol eq-Fe L^{-1} (n = 201; Figures 2A–4A). The lowest concentration was measured at station 6 at 920 m and the highest concentration was detected at station 8 at 25 m in the South Pacific Gyre. At each station, the vertical distribution was similar (Figure 2A) with high concentration (> 1 nmol eq-Fe L^{-1}) in the upper 55 m (Figure 2A) decreasing with depth in the mesopelagic waters to a relative minimum (L$_{FeHS}$< 0.2 nmol eq-Fe L^{-1}) generally observed between 500 and 1500 m. In the abyssal waters, L$_{FeHS}$ increased, reaching concentrations close to 0.5 nM eq-Fe (Figure 2A). The interval of concentration and the vertical distribution we report in this work are in good agreement with previous studies reporting humic-type ligand concentrations, including those from the southwestern Pacific (Cabanes et al., 2020). L$_{FeHS}$ concentrations in the different water masses identified by the OMP are presented Table 1. AAIW was the most depleted (mean$_{AAIW}$ = 0.33 ± 0.16 nmol eq-Fe L^{-1} n = 41) and LCDW the most enriched (mean$_{LCDW}$ = 0.55 ± 0.31 nmol eq-Fe L^{-1} n = 9) in L$_{FeHS}$. Titration of iron-binding ligands (L$_{Fe}$) over 103 samples provide the complexing capacity of dissolved organic matter for Fe (Figure 2B). L$_{Fe}$ ranged from 2.8 ± 0.4 to 9.3 ± 1.0 nmol eq-Fe.L^{-1} with a mean concentration of 5.2 ± 1.2 nmol eq-Fe.L^{-1}. The distribution of L$_{Fe}$ was relatively homogenous along the water column (Figure 2B). The contribution of L$_{FeHS}$ to L$_{Fe}$ was calculated as the ratio between both parameters. Among the 103 samples investigated, L$_{FeHS}$ contributed to between 2% and 51% of L$_{Fe}$ (Figure 2C) with a mean of 11 ± 8%. The ratio of LFeHS over DFe (Figure 2D) exhibited a wide range of values, spanning from<0.1 to 15.4, with an average of 1.3 ± 1.8. Half of the samples had a ratio below 1, indicating that the organic complexation of DFe by L$_{FeHS}$ cannot explain alone the observed ambient DFe concentrations along the section. Lower values were observed in the LD5 samples and in
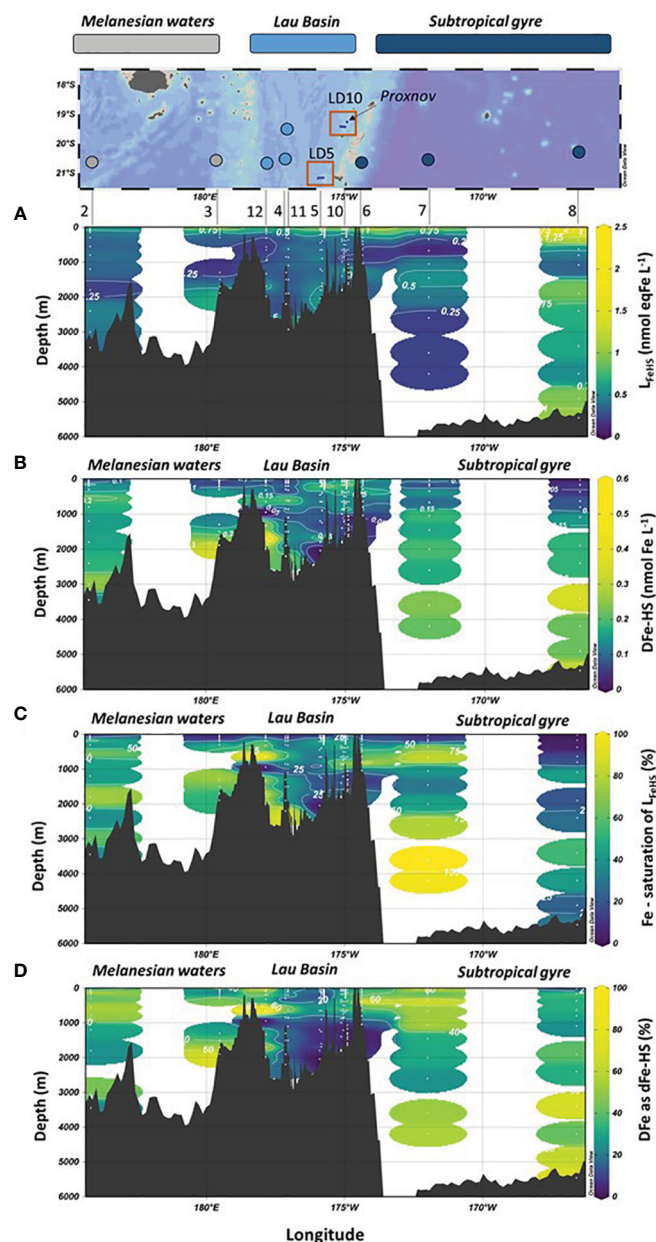
FIGURE 3

Vertical distribution of **(A)** Iron binding ligands of humic nature (L$_{FeHS}$); **(B)** dissolved iron (DFe) effectively complexed by L$_{FeHS}$ (DFe-HS); **(C)** L$_{FeHS}$ saturation state (%); **(D)** Percentage of DFe under DFe-HS (%) with longitude during the TONGA expeditione (GEOTRACES GPpr14). Map of the expedition and the three distinct biogeochemical domains crossed are indicated.

the samples collected in the PDW, while higher values were observed in the surface samples and in the LCDW.

3.3 Iron associated with L$_{FeHS}$ and L$_{FeHS}$ saturation state

The concentration of Fe complexed by L$_{FeHS}$ was estimated by considering the saturation state of L$_{FeHS}$ and the binding capacity (BC) of the external standard used (SRFA 1S101F; BC$_{SRFA}$ = 14.6 nmol Fe. mg SRFA^{-1}, Sukekava et al., 2018). Despite the uncertainty of this methodology (see section 2.3), it provides information regarding the amount of DFe associated to L$_{FeHS}$. The average calculated DFe-HS was 0.15 ± 0.10 nmol Fe L^{-1} (n = 192) and ranged between 0.03 ± 0.02 nmol Fe L^{-1} to 0.56 ± 0.04 nmol Fe L^{-1}. The mean contribution of DFe-HS to DFe was 30 ± 23%. The lowest concentrations were found between depths at depths between 60 and 120 m for four stations (Figures 3C, 4). The highest
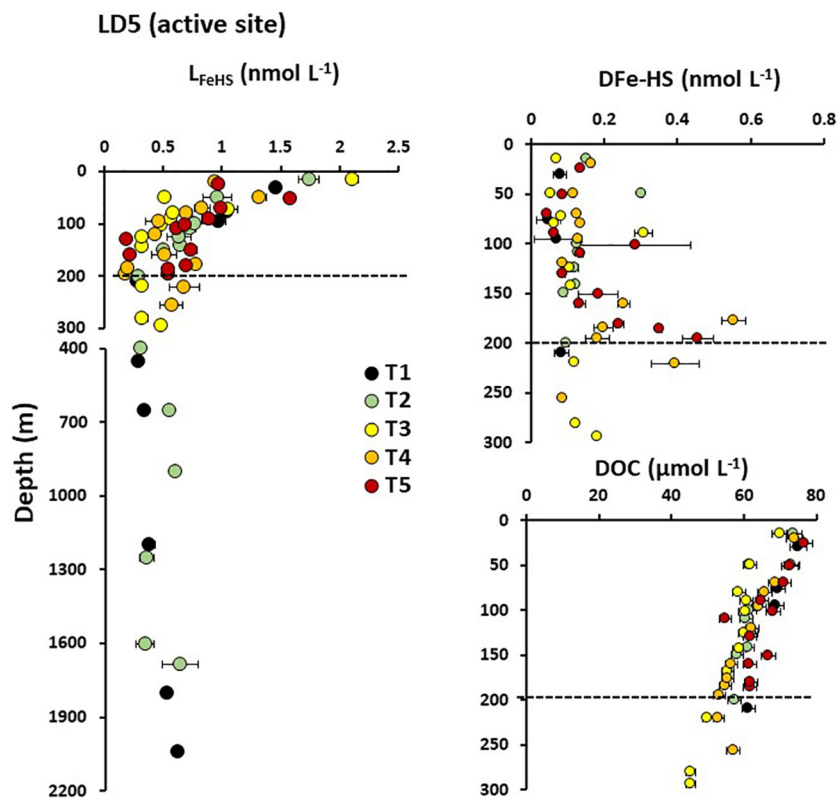
FIGURE 4

Vertical distribution of humic-type ligand concentrations (L_{FeHS}) above and in the vicinity of LD 5 hydrothermal site. Dashed lines indicate the approximate depth of the hydrothermal plume at LD 5-T5 (~190 m). Associated concentrations of dissolved iron complexed by L_{FeHS} (DFe-HS) and of dissolved organic concentrations (DOC) are presented for the upper 300 m.

concentration was recorded at 175 m of substation T4 of LD5 in the vicinity of the hydrothermal plume of LD 5 (Figure 4A). In this latter sample, a DFe peak (~10 nM) associated with hydrothermal activity was recorded by Tilliette et al. (2022) and DFe-HS contributing for 5.5% of total DFe. DFe-HS concentrations were generally lower than 0.2 nmol L^{-1} in the upper 200 m, with the exception of LD 5 and LD 10 (Figure 4), and higher than 0.2 nmol L^{-1} in the intermediate and deep waters (deeper than 1000 m, Figure 3). The local minima of DFe-HS were generally observed at the depth of the local Chlorophyll maxima (see section 4.4). At these depths DFe-HS accounted for 21 ± 15% of total DFe. The saturation of L_{FeHS} by Fe is presented in Figure 3D. With the exception of one datapoint at 3500 m at station 7, ambient L_{FeHS}

were not saturated by Fe. The mean saturation state was 37 ± 26% (n = 192), ranging from 3 ± 5% at 25 m at station 8 to up to 102 ± 4% at 3600 m at station 7. Lowest saturation states (< 10%) were found in the upper water, associated with low DFe concentrations (SD 3, 7, 8). This was expected considering the low DFe concentrations (Tilliette et al., 2022) and the high L_{FeHS} concentrations (Figure 3A). In the Lau Basin, relatively low saturation states of L_{FeHS} (< 30%, Figure 3D) were observed between 1000 and 1400 m depth. Deeper than 1000 m depth, the saturation of L_{FeHS} was generally higher than 40% in the Melanesian waters and the south Pacific subtropical gyre. Our results indicate that a large fraction of L_{FeHS} were not saturated by Fe. These free L_{FeHS} should be able to support Fe complexation and its

TABLE 1 Mean concentration of iron binding ligands of humic nature (L_{FeHS}) and associated variability (SD) measured in the water masses encountered during the TONGA expedition.

	STUW	WSPCW	AAIW	PDW	LCDW
Depth range (m)	[100-300]	[300-500]	[500-1300]	[1300-3000]	> 3000
Mean L_{FeHS} (nmol eq-Fe L^{-1})	0.48	0.37	0.33	0.42	0.55
SD (nmol eq-Fe L^{-1})	0.24	0.22	0.16	0.19	0.31
n	60	18	41	34	9

See text for abbreviations of water masses.

stabilization in the dissolved phase if Fe is added to the system by volcanic or hydrothermal activity.

3.4 L_{FeHS} and DFe-HS in a hydrothermal system of the Tonga arc

The impact of the hydrothermal activity along the Tonga arc on L_{FeHS} concentrations and DFe associated with these ligands (DFe-HS) was studied at LD 5 and LD 10. Five and four subcasts were operated at LD 5 and LD 10, respectively, to capture the dispersion of the hydrothermal plume. We focus here on the active site LD5 (Figure 4) where high DFe concentrations (up to 50 nmol L^{-1}) were measured close to the vent (Tilliette et al., 2022). At the subcasts close to the vent (T5 and T4), L_{FeHS} and DOC concentrations did not show any significant enrichment at depths where the hydrothermal plume was located (~195 m; Figure 4). Similarly, there was no L_{FeHS} or DOC enrichment at LD 10 (see Supplementary Information). These results indicate that these hydrothermal systems were not a source of L_{FeHS} or DOC. In contrast, DFe-HS did show an enrichment at depths where the hydrothermal plume was located (Figure 4B). At T5, the concentration of DFe-HS increased while the saturation of L_{FeHS} decreased with increasing proximity to the vent, from 0.06 nmol L^{-1} (8% saturated with Fe) at 70 m to 0.46 nmol L^{-1} (83% saturation) at 195 m depth, nearest the vent. Due to the much higher DFe concentration in the deeper sample (DFe ~50 nmol L^{-1} at 195m), only ~1% of DFe was complexed by L_{FeHS} at this depth. The highest DFe-HS concentration was measured at 175 m depth of T4 (0.56 nmol L^{-1}) where DFe was ~10 nmol L^{-1} with ~5.5% of DFe was present under DFe-HS. Unsaturation of L_{FeHS} at 195 m of T5 despite the high DFe concentration (~ 50 nmol L^{-1}) suggests that this hydrothermal DFe was present under a chemical form not fully accessible for complexation by L_{FeHS}. The increase in DFe-HS concentration during plume dispersion between T5 and T4 (Figure 4B) indicates that complexation of DFe by L_{FeHS} begins at the onset of hydrothermal mixing and proceeds further during plume dispersion. Our data thus indicate that the complexation of hydrothermal DFe by L_{FeHS} is a kinetically controlled process.

3.5 Iron oxyhydroxide dissolution by humic-type ligands: from lability to inertness

Hydrothermal systems release large amounts of FeOx to the ocean, thereby we studied the ability of L_{FeHS} to solubilize FeOx in seawater. For this purpose, a dissolution experiment of FeOx in the presence of a model L_{FeHS} (SRFA) was carried out (Figure 5A). The experiment consisted of monitoring the formation of the DFe-HS as a function of time and as a function of age of FeOx. Results show that immediately after FeOx formation, amorphous Fe(III) is accessible to L_{FeHS} generating a quantifiable signal. Within an hour, 40% of initially-formed FeOx were dissolved, demonstrating that L_{FeHS} can solubilize FeOx with a kinetic rate constant (k) of at least 1.2 10^6 mol^{-1} L min^{-1}.

Age of FeOx was however a strong controlling parameter on the dissolution rate. A dramatic linear decrease of k with time (k = 1.25 10^6 M^{-1} - 0.18 * t(d), R^2 = 0.99, n = 10) was observed (Figure 5B). After 2 days only 2.5 nmol L^{-1} over 10 nmol L^{-1} of FeOx can be dissolved by SRFA after 1 hour of experiment. After a week of ageing, there was no quantifiable signal after 1 hour experiment (Figure 5A). Additional experiments were carried out two weeks after FeOx formation and no measurable signal was observed (data not shown).

4 Discussion

4.1 L_{FeHS} cycling in the WTSP

The high concentrations and surface maxima of L_{FeHS} observed in this area not impacted by continental inputs indicate a marine origin of L_{FeHS} in these subtropical waters. Direct excretion by phytoplankton is a possible source of L_{FeHS} (Stedmon and Cory,
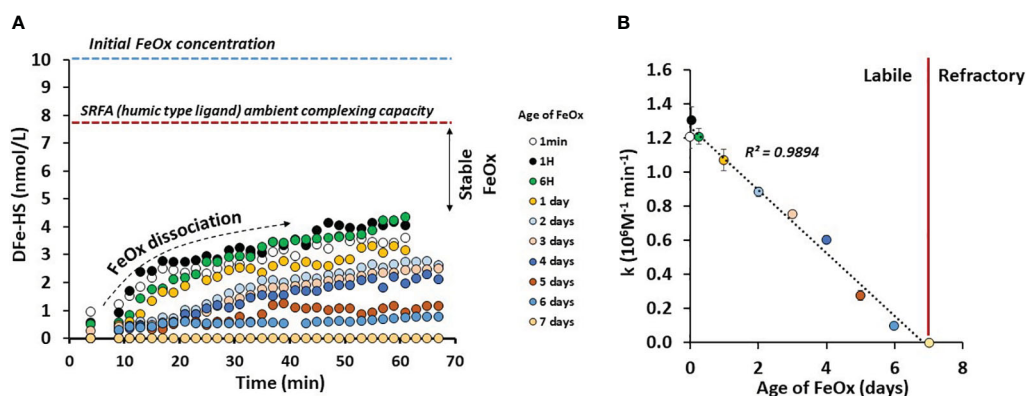

FIGURE 5
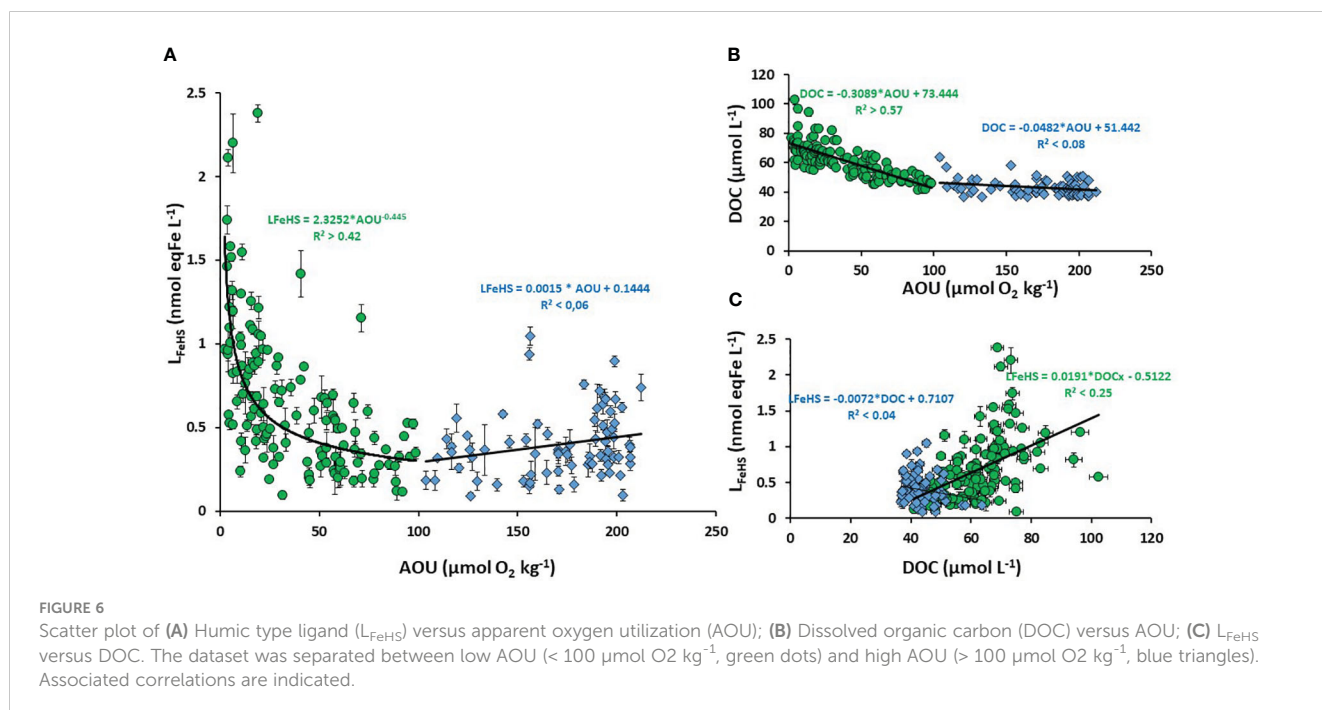**(A)** [Fe] (nmol kg^{-1}) bound by a humic-type ligand (SRFA 1S101F) as a function of time (min) and age of iron oxyhydroxide (FeOx) in artificial seawater.
(B) Dissolution rate constant of FeOx (k in µM^{-1} min^{-1}) as a function of FeOx ageing. See text for explanations.

2014), however chlorophyll *a* (derived from CTD fluorescence sensor) and L_{FeHS} discrete maxima were not observed at the same depth (see section 4.4). The absence of a significant correlation between chlorophyll *a* and L_{FeHS} in the upper 200 m ($R^2 < 0.1$; $p > 0.75$, n = 91) suggest an indirect pathway for the production of these ligands. The release of DOM during the degradation of phytoplankton material (cell lysis, grazing) in the first hundred meters combined with its microbial and chemical processing (Obernosterer et al., 1999) are the most probable pathway of production for these ligands. This proposed production pathway is in agreement with *in situ* experiments from Whitby et al. (2020a) who showed a release of humic-type ligands during microbial respiration of biogenic particulate organic carbon originating from the oligotrophic Mediterranean waters and from the high nutrient low chlorophyll Southern Ocean waters.

The vertical decrease of L_{FeHS} in the mesopelagic zone (Figures 2A, 3A) reveals the partial degradation of L_{FeHS} during microbial mineralization of DOM. Direct consumption of humics by heterotrophic bacteria reported in several studies (Cottrell and Kirchman, 2000; Coates et al., 2002; Rosenstock et al., 2005) support our observations. The persistence of L_{FeHS} in the deep PDW (mean$_{PDW}$ = 0.43 ± 0.19 nmol eq-Fe L^{-1} n = 34) indicate that part of L_{FeHS}, however, escapes microbial degradation and is refractory. To monitor the effect of microbial mineralization process on L_{FeHS}, we calculated the apparent oxygen utilization (AOU) based on dissolved oxygen concentrations, S, T (all derived from CTD sensors) using Benson and Krause (1984) formula. AOU is the integrated oxygen consumption by heterotrophic bacteria in the breakdown of organic matter. In the study area, mineralization of labile, semi-labile and semi-refractory DOM can be tracked by the linear decrease of DOC concentration (i.e. proxy of DOM) with increasing AOU down to ~100 μM ($R^2 > 0.57$; $p < 0.05$; n = 133; Figure 6B). At AOU > 100 μmol O_2 kg^{-1}, DOC concentrations were

relatively homogenous (~ 37 μM) indicating that DOC was mostly refractory to microbial respiration. A plot of L_{FeHS} against AOU also reveals a decrease of humic-type ligand concentration during the mineralization process (Figure 6B). Down to an AOU of 100 μmol O_2 kg^{-1} the decrease of L_{FeHS} was likely driven by a power law ($R^2 > 0.42$; $p < 0.05$; n =133) rather than by direct linear regression. At AOU > 100 μmol O_2 kg^{-1}, L_{FeHS} seems to increase with increasing AOU (Figure 6A) but the correlation was not significant ($R^2 < 0.05$; $p > 0.05$; n = 75). A weak but significant correlation between L_{FeHS} and DOC for AOU > 100 μmol O_2 kg^{-1} (Figure 6C; $R^2 > 0.25$; $p < 0.05$; n = 133) was observed indicating that L_{FeHS} cannot be modeled accurately through an empirical equation based on DOC. The weak correlation between L_{FeHS} and DOC was expected due to the intrinsec difference between both parameters. On the one hand, DOC consists of a broad pool of molecules that undergo both respiration-driven losses and gradual conversion into refractory compounds (Figure 6B). On the other hand, L_{FeHS} represents a more specific property (binding sites) of DOM that is primarily lost through microbial turnover (Fourrier et al., 2022).

The contribution of L_{FeHS} to L_{Fe} in our study (2% to 51%, Figure 2) is lower compared to the findings of Whitby et al. (2020b) (23-58%) in the North Atlantic Ocean. This disparity can be attributed to both geographical and methodological differences. Whitby et al. (2020b) studied samples from the North Atlantic Ocean, where the presence of terrestrial influence (and the associated humic substances) could potentially lead to high concentrations of L_{FeHS}. In contrast, the study area of the WTSP lacks terrestrial influence, resulting in the absence of a terrigenous component and lower concentrations of L_{FeHS} than in the Atlantic. Furthermore, our study used SA as the competing ligand for L_{Fe} titration, while Whitby et al. (2020b) used 2-(2-Thiazolylazo)-p-cresol (TAC). It is important to note that TAC may not fully capture the contribution of humic-type ligands (as highlighted by Laglera

FIGURE 6
Scatter plot of **(A)** Humic type ligand (L_{FeHS}) versus apparent oxygen utilization (AOU); **(B)** Dissolved organic carbon (DOC) versus AOU; **(C)** L_{FeHS} versus DOC. The dataset was separated between low AOU (< 100 μmol O2 kg^{-1}, green dots) and high AOU (> 100 μmol O2 kg^{-1}, blue triangles). Associated correlations are indicated.

et al., 2011 and Slagter et al., 2019). Therefore, the values reported by Whitby et al. (2020b) might represent the minimum concentration of the ligand pool, underestimating the actual presence of humic substances. These factors account for the higher L_{FeHS} contribution reported by Whitby et al. (2020b) in the North Atlantic compared to our study.

4.2 Classification of L_{FeHS} and iron speciation within L_{FeHS} in the western Pacific Ocean

The L_{FeHS} concentrations measured during this study were lower than the total iron binding ligand (L_{Fe}) concentration measured by CLE-CSV (Figure 2). Over the 103 common samples analyzed by CLE-CSV and L_{FeHS}, the mean log $K_{FeL,Fe'}^{cond}$ was 11.6 ± 0.4 ranging from 10.5 ± 0.2 to 12.7 ± 0.3. According to the classification defined by Gledhill and Buck (2012), 84% of samples fall in the L_2 class, 13% in the L_1 class, and 4% in the L_3 class (Mahieu et al., this issue). This result clearly indicate that intermediate class ligands (L_2) dominated the pool of L_{Fe} all along the water column in our study area. This is in agreement with the previous datasets reported by Buck et al. (2018) and Cabanes et al. (2020) in the oligotrophic South Pacific Ocean. Cabanes et al. (2020) also measured L_{FeHS}, and showed that the weakest class of ligand (log $K_{FeL,Fe'}^{cond}$ < 11) observed was associated with the lowest humic-type ligand concentration. All these observations indicate that the L_{FeHS} measured here are ligands of intermediate strength (L_2 type). However, classifying based on log $K_{FeL,Fe'}^{cond}$ does not capture the heterogeneity of binding sites for non-discrete ligands like L_{FeHS}. To mitigate biases introduced by CLE-CSV, it is preferable to use $\alpha FeL(Fe')$ (reactivity coefficients) for studying the nature of LFe (Gledhill and Gerringa, 2017).

To study the nature in term of strength of L_{FeHS}, we conducted competitive ligand experiments for Fe complexation between ambient natural ligand including L_{FeHS} and Gallic Acid (GA) to study the mobility of Fe and its speciation within the Fe-humic complex. According to the only available published data from González et al. (2019), GA in seawater is a weak Fe ligand (log K_{FeGA} = 9.1) with a binding capacity of 2.75 nmol eq-Fe nmol GA^{-1}. We choose this ligand for two reasons. Firstly, GA is a polyphenolic compound with a carboxylate moiety. Phenolic and carboxylates are thought to be the moieties involved in the formation of the Fe-humic complex (Garnier et al., 2004; Hassler et al., 2019). GA is thus a good candidate to compare the affinity of Fe for humic substances with these moieties. Secondly, GA reduces Fe(III) into Fe(II) with time (González et al., 2019; Pérez-Almeida et al., 2022). The affinity of marine humic type ligand for Fe(II) can then be studied after i) the saturation of GA with Fe, ii) equilibrium to allow the reduction of Fe(III) into Fe(II) by GA, and competition ligand experiment.

The sample used for this experiment has an initial DFe concentration of 0.45 ± 0.01 nmol L^{-1}; L_{Fe} was 4.8 ± 0.5 nmol eq-Fe L^{-1} with an associated log $K_{FeL,Fe'}^{cond}$ of 11.8 ± 0.4 (Mahieu et al., this issue). L_{FeHS} was estimated at 1.52 ± 0.02 nmol eq-Fe L^{-1}, 32% of L_{Fe}. The initial DFe-HS was 0.18 nmol L^{-1}. If we consider all DFe to

be labile for organic complexation, the initial conditions of the experiment can be described as follows: (i) L_{Fe}' and L_{FeHS}' were respectively 4.3 and 1.34 nmol eq-Fe L^{-1}, (ii) 0.27 nmol L^{-1} DFe were complexed by non-humic L_{Fe} and (iii) the log $\alpha FeL(Fe')$ (e.g. side reaction coefficient) was 3.4. A first experiment consisted of the addition of 1.6 nmol L^{-1} of Fe to the sample. After 20 h of equilibration, DFe-HS reached 1.50 ± 0.05 nmol L^{-1} thereby L_{FeHS} were at saturation. Considering the ambient L_{Fe} concentration of the sample, determined by CLE-ASV, our results demonstrate that the Fe added went primarily into L_{FeHS}. CLE-ACSV analysis only provides an average lo $K_{FeL,Fe'}^{cond}$ g of the ligand pool (captured by the detection window of the method) but the L_{Fe} pool is composed of a wide variety of organic compounds with different log $K_{FeL,Fe'}^{cond}$ (Town and Filella, 2000). The log $K_{FeL,Fe'}^{cond}$ of 11.8 ± 0.4 measured for the sample studied is an average of the ligand pool that is composed of ligands and binding sites with both higher and lower strength than this average value.

Considering the initial conditions, it can be inferred that approximately 0.43 nmol eq-Fe L^{-1} of the L_{Fe} pool, including 0.18 nmol eq-Fe L^{-1} of L_{FeHS}, have log $\alpha FeL(Fe')$ values higher than 3.4, indicating the potential presence of L_1 type binding sites (estimated mean log $K_{FeL,Fe'}^{cond}$ ≥ 12.8). Since the addition of DFe initially fills the remaining free sites of L_{FeHS}, our results suggest that the log $\alpha FeL_{FeHS}(Fe')$ values for the binding sites in L_{FeHS} that were not initially filled with DFe are at least equal to 3.4 (estimated mean log $K_{FeL,Fe'}^{cond}$ ≥ 12.3). Based on the initial conditions and the results of our experiment, a distribution of binding site density within the L_{FeHS} pool can be inferred. L_{FeHS} comprises a small portion (12%) of sites with high affinity (L_1 type) that can outcompete strong discrete ligands, while the majority (88%) of sites fall into the L_2 type category, likely at the higher end of the strength scale associated with L_2 type sites. The remaining 3 nmol eq-Fe L^{-1} of the L_{Fe} pool may be considered as weaker ligands compared to L_{FeHS}. Our findings are consistent with the results reported by Gledhill et al., 2022, who demonstrated that the heterogeneity of binding sites in humic-like DOM enables humic substances to outcompete siderophores at low iron concentrations.

In a second experiment, Fe-free GA was added but the response of DFe-HS was unchanged, showing that the Fe cannot be dissociated from the Fe-humic complex by 2 nmol L^{-1} of GA (L_{FeGA} = 5.5 nmol eq-Fe.L^{-1}) at a pH of 8.0 (Figure 7). This demonstrate that the affinity of L_{FeHS} for Fe is higher than $10^{9.1}$ and that polyphenolic and carboxylate moieties of GA cannot outcompete those involved in the complexation of Fe in L_{FeHS} even at higher GA ligand concentration. This experiment confirms that surface L_{FeHS} in the WTSP are, at least, ligands of intermediate strength.

In a third experiment, 2 nmol L^{-1} of GA saturated with Fe were put in contact with unsaturated L_{FeHS} (Figure 7). After 20 h of equilibration, L_{FeHS} were able to dissociate partly Fe from the Fe-GA complex. However L_{FeHS} but did not reach saturation even with an addition of 5.5 nM of DFe bound to GA (e.g. 5.5 nmol eq Fe L^{-1} for 2 nmol L^{-1} GA; González et al., 2019). Using equations (2) to (8), this scenario allows to calculate the apparent stability constant of L_{FeHS} in the condition of the experiment (20°C, pH = 8, 20h of competition). A value of $logK_{LFeHS}$ = 8.5 ± 0.2 was obtained, much
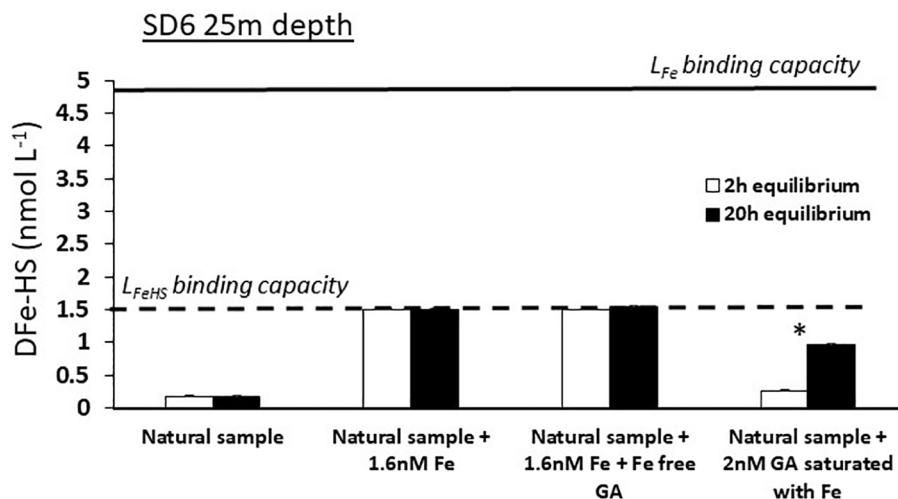
FIGURE 7
Monitoring of dissolved iron complexed by humic type ligand concentration (DFe-HS) before (white bars) and after(dark bars) overnight equilibration between natural ambient iron-binding ligands (L_{Fe}), humic-type ligands (L_{FeHS}) and Gallic Acid (GA) for a surface sample with oligotrophic conditions (SD 6, 25 m depth). Solid and dashed line indicate the iron binding capacity of the ambient L_{Fe} and L_{FeHS}. * indicates a significant difference between initial and final DFe-HS concentrations. Absence of iron saturation of L_{FeHS} in experiments c and c' and no changes in DFe-HS in experiments d and d' indicate the instability of Fe(II)-humic ligand complexes and that Fe(III)-humic complexes are of higher stability than Fe-GA complexes. See text for explanation.

lower than expected from the first two experiments. There are various possibilities to explain these apparent differences:

i) the third experiment was not at equilibrium and the reaction need to be longer than 20h; this hypothesis was disproved by running a similar experiment but with 36h equilibration time; same results were obtained. ii) The Fe-humic complex is metastable and cannot be dissociated even by a stronger ligand; this is unlikely from previous experiments conducted by Laglera et al. (2019) who demonstrated that desferrioxamine B (strong ligand) and EDTA (weak ligand) can both dissociate Fe from a natural Fe-humic complex when their concentrations are sufficiently high. iii) GA partially reduced Fe(III) to Fe(II), because the latter has higher affinity for GA and non-humic L_{Fe} than Fe(III) has for L_{FeHS}, resulting in an apparent lower log $K_{FeL,Fe'}^{cond}$. The pH dependence of the Fe-humic reduction peak potential (increasing peak potential E_{peak} with decreasing pH) observed by Laglera et al. (2007) provide further perspectives for interpretation iii). Their observations indicate that the stability of the Fe-humic complex decreases with decreasing pH. An increasing proportion of Fe(II) at lower pH can explain this shift of E_{peak} with pH, since Fe (II)-humic complexes have lower stabilities compared to Fe(III)-humic complexes (Rose and Waite, 2003a; Blazevic et al., 2016). Based on our experiments and the studies mentioned above, we suggest here that a Fe-humic complex is only stable in seawater with Fe(III). It can be further hypothesized that to form an Fe-GA complex stable in seawater, Fe should be under Fe(II) in the Fe-GA complex. These conclusions have broader implications for the fate of Fe in environments with low pH and changing redox conditions, such as low oxygenated margins and hydrothermal environments (as observed at LD5 T5, Figure S4), or where photoreduction of Fe is enhanced (e.g. clear subtropical waters).

4.3 The role of L_{FeHS} in the stabilization of hydrothermal DFe

The kinetic monitoring of FeOx dissolution by L_{FeHS} demonstrates that the age of FeOx is a main factor controlling their dissolution rate (Figure 5). The experiment we conducted shows that recently formed FeOx are very labile but become gradually refractory to dissolution by L_{FeHS} with time; the studied model humic-type ligand was not able to solubilize FeOx aged one week or more (Figure 5). A similar effect of ageing on the solubilization of FeOx was observed for desferoxiamine B (Rose and Waite, 2003b) with a nearly 50 times decrease of the dissolution rate constant after a week of FeOx maturation. Our results are also in line with those of Krachler et al. (2015) who observed a rapid dissolution of newly formed FeOx by a set of L_{FeHS} and experiments by Tani et al. (2003) that correlated the solubilization of newly formed FeOx with humic-like fluorescence in seawater. In contrast, Kuma et al. (1996) did not see such a strong effect of age on FeOx solubility probably due to inherent differences in methodologies. They added FeOx in natural seawater and followed their solubility over time, which is equivalent to studying the stability of organically complexed DFe originating from the dissolution of newly formed FeOx.

In hydrothermal environments, most DFe is released under the form of soluble Fe(II). The fraction of DFe that escapes precipitation of sulfide minerals (e.g. pyrite, chalcopyrite) is then gradually oxidized and forms insoluble Fe (III) oxyhydroxides species (FeOx) both under colloidal and particulate form (Lough et al., 2019; Cotte et al., 2020; Hoffman et al., 2020). Recent studies highlight the high proportion of colloidal DFe in hydrothermal plume at dozens to hundreds of kilometers from the vent (Tagliabue

et al., 2022; Lough et al., 2023). However the persistence of DFe plumes at great distances from deep vents is often explained by its initial stabilization under an organic form (Sander and Koschinsky, 2011; Hawkes et al., 2013; Wang et al., 2021; Wang et al., 2022). In the first stage of hydrothermal mixing, DFe occurs essentially as Fe (II) species (Waeles et al., 2017). With Fe(II) having low affinity for L_{FeHS}, (Figure 7; Rose and Waite, 2003a), the pathway of Fe-HS formation in hydrothermal plumes requires the oxidation of Fe(II) to Fe(III), through the formation of colloidal Fe oxides species that may be partly dissolved by L_{FeHS}. Our experiments strongly suggest that dissolution of FeOx by humic-type ligands is only possible during the first hours or days after precipitation (Figure 5). Ligand concentration is not the only factor controlling the solubility of FeOx as shown by our lab experiments and field observations (unsaturated L_{FeHS} in the presence of high DFe concentrations, Figure 4). Therefore, the kinetics of the plume dispersion must be taken into account when studying the organic complexation of hydrothermal Fe. The persistence within the DFe fraction of colloidal FeOx observed in the widespread hydrothermal plume of the Pacific Equatorial Ridge (Fitzsimmons et al., 2017) is in agreement with our observations and support our conclusions. It is worth noting that our dissolution experiments were achieved in UV digested artificial seawater, neglecting key parameters of the hydrothermal environment (e.g. pH, O_2, pressure, temperature, DOC, sulfide, other trace metals) that may impact the nature, concentrations, kinetics of formation, stability and transport of these Fe colloidal species. For instance, the composition of the fluid, dissolved O_2 concentrations, pH, temperature and local currents driving plume dilution are parameters to be considered for Fe oxidation and mineral formation (Byrne et al., 2000; Field and Sherrell, 2000; Shaw et al., 2021; Tilliette et al., 2022). Although not representative of the natural hydrothermal system, our dissolution kinetics experiments provide valuable insights into the processes involved.

At LD5, we observed that L_{FeHS} stabilized a very small fraction of the DFe released by the hydrothermal vent (Figure 4) keeping unsaturated L_{FeHS} in the presence of high DFe (~50 nmol L^{-1}). This inability of L_{FeHS} to complex DFe released at LD5-T5 might be due to the low pH (< 6.5) and low O_2 (< 160 μM) values at this site, resulting in a seawater relatively acidic and suboxic (Tilliette et al., 2022; Figure S4). Under these conditions, a significant fraction of Fe (II) may persist which has low affinity for L_{FeHS}. In addition, the fraction of DFe stabilized by L_{FeHS} increased from 1 to 5.5% between substations T5 and T4 while a majority (78%) of the DFe released precipitated in the first 600 m (Tilliette et al., 2022). During its dispersion in shallow waters, the plume is rapidly diluted with more alkaline, more oxygenated and warmer seawater that will favor the formation of FeOx species (Figure S4). This newly formed FeOx may be dissolved by L_{FeHS} (Figure 5) at a rate that is at least dependent on the age of these FeOx as well as the concentration of Fe-free L_{FeHS} (Figure 5) and certainly on many other parameters (concentration of particles, concentration of other dissolved metals, DOC, plume dispersion, etc). It is worth noting that pH and temperature play crucial roles in iron organic complexation and FeOx formation (Byrne et al., 2020; Ye et al., 2020; Zhu et al., 2021). Considering the significant variations in these parameters within

hydrothermal environments (Figure S4), it is recommended to design further experiments to gain a better understanding of the impact of pH and temperature on the dissolution of FeOx by L_{FeHS}.

4.4 Bioavailability of DFe-HS and stabilization of DFe by L_{FeHS} in intermediate and deep waters of the WTSP

For data interpretation, samples with DFe concentrations exceeding 2 nnmol L^{-1} were identified as being influenced by the hydrothermal system and were subsequently excluded from the depth horizons discussed in the following sections. In the first 50 m of the water column, above the deep chlorophyll maximum (Above DCM, Chl $a < 0.075$μg L^{-1}), L_{FeHS} was high (mean$_{Above DCM}$ $L_{FeHS} > 1.2 \pm$ nmol eq-Fe L^{-1} n = 18; Figure 8A) and DFe-HS concentrations were relatively low (mean$_{Above DCM}$ DFe-HS = 0.18 ± 0.12 nmol L^{-1} n = 18; Figure 8B) resulting in a low saturation of L_{FeHS} (17 ± 10%, n = 18 Figure 8C). The non-accumulation of DFe in the presence of high L_{FeHS} is in stark contrast with what was observed in the Mediterranean Sea (Dulaquais et al., 2018a) and in the Arctic waters (Laglera et al., 2019). This observation suggests that, in the surface water of the WTSP, DFe can be dissociated from the humic complex, becoming available for surface reaction (e.g. scavenging) or biological uptake. It is not clear from our data if DFe is directly removed from the humic complex or if photoreduction of Fe within the complex via ligand-to-metal charge transfer leads to the production of Fe(II) with low affinity for L_{FeHS} (Figure 5; Barbeau, 2006; Blazevic et al., 2016). An additional process explaining the non-accumulation of DFe within L_{FeHS} in surface could be the presence of DFe under a colloidal fraction that is not available for complexation with L_{FeHS}. Colloidal DFe can represent a large fraction of DFe in surface waters of the Pacific ocean (Wu et al., 2001). It is considered poorly bioavailable (Rich and Morel, 1990; Chen and Wang, 2001; Wang and Dei, 2003) but prone to scavenging, limiting its accumulation in surface waters (Kunde et al., 2019). Below 50 m depth, a clear and significant ($p < 0.05$) depletion of DFe-HS in the deep chlorophyll maximum (DCM, Chl $a > 0.1$ μg L^{-1}) over the entire section was observed (mean$_{DCM}$ DFe-HS = 0.11 ± 0.08 nmol L^{-1} n = 49; Figure 8). These very low DFe-HS concentrations clearly indicate that when complexed to L_{FeHS}, DFe is bioavailable for phytoplankton. However, it is unclear if phytoplankton cells can directly uptake Fe from the humic complex, if phytoplankton species produce specific ligands to outcompete L_{FeHS} (e.g. EPS, siderophores) or if Fe uptake by the cell is due to remineralisation of the humic-complex (Figure 8). Hassler et al. (2019) classify the model L_{FeHS} SRFA as a source of bioavailable Fe for a set of phytoplankton species but this has not yet been shown, and laboratory culture experiments should be designed to address these questions of DFe-HS bioavailability that could also arise from the dissociation of DFe-HS, as inorganic DFe is continuously assimilated.

Below the DCM (Below DCM, Chl $a < 0.075$ μg L^{-1}; depth > 100m), DFe-HS concentrations was stable (mean$_{Below DCM}$ DFe-HS = 0.15 ± 0.12 nmol L^{-1} n = 38; Figure 8B) and significant ($p < 0.05$)
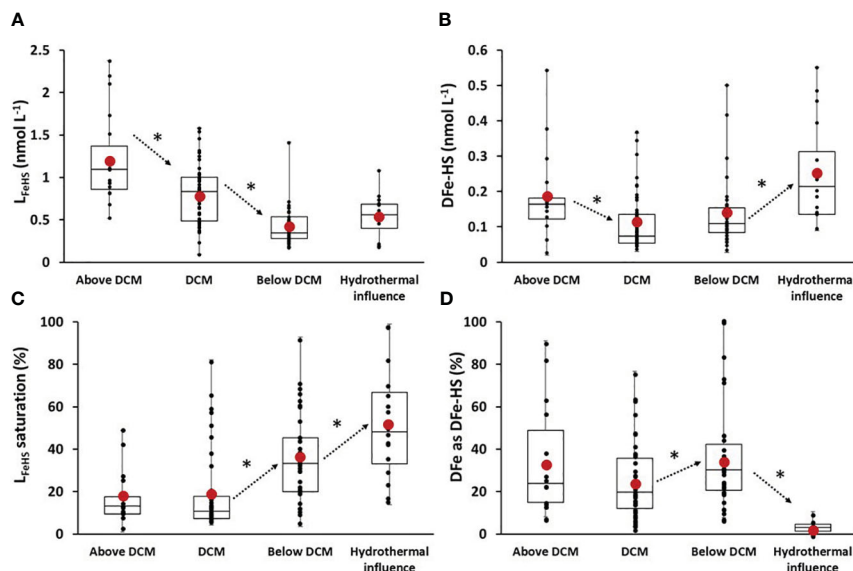
FIGURE 8
Box and whisker plot of **(A)** associated iron binding ligands of humic nature (L_{FeHS} in nmol eq-Fe L^{-1}); **(B)** iron effectively associated with L_{FeHS} (DFe-HS in nmol eq-Fe L^{-1}); **(C)** L_{FeHS} saturation state (%); **(D)** Percentage of DFe under DFe-HS (%) along the section for 4 specific depths clusters of sample: above the deep chlorophyll maximum (above DCM), the deep Chlorophyll maximum (DCM), below the deep chlorophyll maximum and for samples influenced by hydrothermalism. Black dots represent discrete data. Red dots indicate the mean value of data. * and arrows indicate significance and way of variation between two close depth horizons. Significance were tested using Wilcoxon-Mann Whtiney tests and set for 95% of confidence ($p < 0.05$) determined by Wilcoxon-Mann Whtiney test.

increase of L_{FeHS} saturation index (Figure 8C) indicate a stabilization of DFe by L_{FeHS} after the remineralization of sinking biomass. The contribution of DFe-HS to DFe also increase at these depths (Figure 8D), with the exception of LD5-T5 and T4 due to high DFe, further showing an increased stabilisation of DFe by L_{FeHS}. It suggests that Fe binding sites of L_{FeHS} can outcompete Fe adsorption during the mineralization of particulate Fe (e.g. scavenging). This observation is in line with the work of Whitby et al. (2020b) that suggest L_{FeHS} concentration as the upper limit on how much remineralized Fe can be stabilized in the dissolved fraction. As discussed previously in Section 5.3, samples impacted by hydrothermalism exhibit notably higher DFe-HS concentrations ($mean_{hydrothermal\ influence} = 0.25 \pm 0.11$ n = 16) and L_{FeHS} saturation levels ($mean_{hydrothermal\ influence} = 52 \pm 27\%$ n = 16). However, due to the elevated DFe concentrations, the contribution of DFe-HS to total DFe decreases significantly ($5 \pm 3\%$, n = 16), and no significant difference in L_{FeHS} was observed between samples below the DCM and those influenced by hydrothermalism (p > 0.05).

Deeper, DFe-HS increased gradually to reach 0.35 nmol L^{-1} in the PDW composite with DFe-HS accounting for 56% of the total DFe in the abyssal waters (deeper than 2000 m; Figure 3). These results show for the first time that a significant part of DFe is complexed by humic type ligands throughout the water column of the oligotrophic Pacific Ocean and lead to new interpretations for Fe-humic interactions.

Rather constant concentrations of DFe-HS in the deep waters (0.2-0.35 nmol L^{-1} deeper than 1500 m, n = 27) suggest that DFe complexed by L_{FeHS} is stable. In the deep ocean, L_{FeHS} protect DFe from scavenging and contribute to increasing DFe residence time, as previously suggested for L_2 type ligands (Hunter and Boyd,

2007). The water-masses encountered at these depths (Figure 1) fill the entire Pacific Ocean. It can be further hypothesized that this deep, stable pool of DFe-HS can fertilize the euphotic layer with bioavailable DFe when it is upwelled to the surface by mesoscale structures in the equatorial area (Hawco et al., 2021) or by deep-ocean ventilation (Tagliabue et al., 2010) in high nutrient low chlorophyll zones.

The co-existence of unsaturated L_{FeHS} and of a DFe pool not complexed to these ligands (Figure 3) indicates that part of DFe escapes L_{FeHS} complexation. At least three hypotheses can be suggested: i) stronger binding sites than those of L_{FeHS} exist within L_{Fe} pool (L_1 type binding sites); ii) other metals fill the binding sites of humic-type ligands (e.g. copper) or/and iii) Fe is in a chemical form (speciation) unavailable for L_{FeHS} complexation. CLE-CSV analyses of 103 samples (Figure 2B) reveal that L_2 type ligands were detected in 84% of the samples (Mahieu et al., this issue). Moreover, experiments conducted in this work likely indicate that L_{FeHS} are in the higher range of Fe-binding strengths for L_2 ligands (see section 4.2) but initial DFe only partly filled L_{FeHS} possibly indicating that strong binding sites co-exist with weak sites in the apparent L_2 pool. Therefore, it is unlikely that high concentrations of L_1 outcompete L_{FeHS} for DFe complexation. However, the presence of L_1-type binding sites at sub-nanomolar concentrations within the diverse pool of heterogeneous ligands can be considered. Humic-type ligands can bind many other metals including dissolved copper (DCu); humics can have similar binding strength for DFe and DCu in seawater leading to competition for humic complexation between these two elements (Abualhaija et al., 2015). Because DCu is accumulated in the deep Pacific Ocean (Ruacho et al., 2020) at higher concentrations than DFe (Buck et al.,

2018), competition probably takes place,promoting the complexation of DCu over DFe by humic-type ligands in this basin.

The speciation of Fe could also partly explain the apparent undersaturation of humic ligands. A recent study conducted by González-Santana et al. (2023) brought attention to the potential underestimation of Fe(II) and its contribution to the dissolved iron (DFe) pool, suggesting that it may account for around 20% of the total DFe. The unsaturation of L_{FeHS} could be attributed to the limited ability of these ligands to form stable complexes with Fe(II). In addition several studies have shown that a significant fraction (up to 50%) of oceanic DFe is present under colloidal form (cFe > 0.02 µm; Nishioka et al., 2001; Wu et al., 2001; Boye et al., 2010; Fitzsimmons and Boyle, 2014; Kunde et al., 2019). Existence of aged colloidal FeOx (Von der Heyden et al., 2012) refractory to L_{FeHS} complexation (Figure 5) is likely to explain the inability of L_{FeHS} to access to DFe. Nevertheless, the evidence for L_{Fe} exceeding cFe (Boye et al., 2010; Fitzsimmons et al., 2015) suggest that cFe is predominantly organic in open ocean waters. The size fractionation becomes a relevant question since marine humic type substances are of low molecular weight (< 10 kDa; Batchelli et al., 2010; Dulaquais et al., 2020; Fourrier et al., 2022) and can pass through the 0.02 µm membrane usually used to operationally separate DFe into the soluble and the colloidal fractions. Because marine soluble ligands have a similar or higher binding strength than colloidal ones (Boye et al., 2010; Fitzsimmons et al., 2015), the occurrence of unsaturated L_{FeHS} we observed can be interpreted as a physical limitation of this ligand type to access colloidal DFe of high molecular weight (0.02-0.45 µm).

5 Conclusions

This study confirms that L_{FeHS} are heterogenous ligands. The Fe binding strength of L_{FeHS} was not directly measured but lab experiments suggest a distribution of binding sites comprising 10% of L_1 type (log $K_{FeL,Fe'}^{cond}$ > 12.8) and 90% of L_2 type site that are in the higher range of the log $K_{FeL,Fe'}^{cond}$ values recognised for L_2 type site (up to 12). L_{FeHS} are primarily produced in the euphotic layer and mineralized during water mass ageing, encompassing partial recalcitrance throughout the water column. These characteristics lead to a complexation of ~30% of total DFe over the transect studied (n = 186) with a higher percentage of complexation in the deepest waters of the Pacific Ocean (~56% of DFe complexed by humic ligands at depths deeper than 2000 m). In this study, we provided field data evidencing the bioavailability of Fe under Fe-HS form in the deep Chlorophyll maximum. Our data also demonstrate the stabilization of Fe in the dissolved phase by L_{FeHS} after biomass remineralization in the mesopelagic waters. We however observed that part of DFe is not accessible to L_{FeHS}, which remain unsaturated. This may result from the inability of L_{FeHS}, predominantly found in the soluble fraction, to access colloidal DFe. In the vicinity of the active shallow hydrothermal sources studied,

the low stabilization yield (1 to 5.5% of total DFe) and the presence of unsaturated L_{FeHS} concomitant with high DFe concentrations (~50 nmol L^{-1}) lead to the assumption of an inaccessibility of Fe(II) and FeOx species to L_{FeHS}. To support this hypothesis, complexation with Fe(II) and dissolution experiments of FeOx were conducted. We conclude Fe(II) has low affinity for L_{FeHS} and that only one week is necessary to make FeOx totally refractory to L_{FeHS} dissolution. Our work suggests inorganic Fe speciation and the kinetics of shallow hydrothermal plume dispersion must be considered in future studies attempting to close the hydrothermal Fe budget.

Data availability statement

The raw data supporting the conclusions of this article will be made available by the authors, without undue reservation.

Author contributions

GD: Conceptualization, Methodology, Investigation, Data curation, Formal Analysis, Data visualization, Writing – original draft, Writing – review & editing, Supervision, Project administration; PF: Data acquisition, Methodology, Data visualization, Writing – original draft, Writing – review & editing. CG: Project administration, Writing – review & editing; LM: Data acquisition, Writing – review & editing; RR: Writing – review & editing; CT: Data acquisition, Writing – review & editing; PS: Writing – review & editing; HW: Writing – review & editing. All authors contributed to the article and approved the submitted version.

Funding

Acknowledgments

Conflict of interest

The authors declare that the research was conducted in the absence of any commercial or financial relationships that could be construed as a potential conflict of interest.

Publisher's note

All claims expressed in this article are solely those of the authors and do not necessarily represent those of their affiliated organizations, or those of the publisher, the editors and the reviewers. Any product that may be evaluated in this article, or claim that may be made by its manufacturer, is not guaranteed or endorsed by the publisher.

Supplementary material

The Supplementary Material for this article can be found online at: https://www.frontiersin.org/articles/10.3389/fmars.2023.1219594/full#supplementary-material

References

Abualhaija, M. M., and van den Berg, C. M. (2014). Chemical speciation of iron in seawater using catalytic cathodic stripping voltammetry with ligand competition against salicylaldoxime. *Mar. Chem.* 164, 60–74. doi: 10.1016/j.marchem.2014.06.005

Abualhaija, M. M., Whitby, H., and van den Berg, C. M. (2015). Competition between copper and iron for humic ligands in estuarine waters. *Mar. Chem.* 172, 46–56. doi: 10.1016/j.marchem.2015.03.010

Barbeau, K. (2006). Photochemistry of organic iron (III) complexing ligands in oceanic systems. *Photochem. Photobiol.* 82 (6), 1505–1516. doi: 10.1111/j.1751-1097.2006.tb09806.x

Batchelli, S., Muller, F. L., Chang, K. C., and Lee, C. L. (2010). Evidence for strong but dynamic iron– humic colloidal associations in humic-rich coastal waters. *Environ. Sci. Technol.* 44 (22), 8485–8490. doi: 10.1021/es101081c

Benner, R. (2011). Loose ligands and available iron in the ocean. *Proc. Natl. Acad. Sci.* 108 (3), 893–894. doi: 10.1073/pnas.1018163108

Benson, B. B., and Krause, D.Jr. (1984). The concentration and isotopic fractionation of oxygen dissolved in freshwater and seawater in equilibrium with the atmosphere 1. *Limnol. Oceanogr.* 29 (3), 620–632. doi: 10.4319/lo.1984.29.3.0620

Blazevic, A., Orlowska, E., Kandioller, W., Jirsa, F., Keppler, B. K., Tafili-Kryeziu, M., et al. (2016). Photoreduction of terrigenous Fe-humic substances leads to bioavailable iron in oceans. *Angew. Chem.* 128 (22), 6527–6532. doi: 10.1002/ange.201600852

Boggs, S. Jr., Livermore, D., and Seitz, M. G. (1985). *Humic substances in natural waters and their complexation with trace metals and radionuclides: a review [129 references].* United States. doi: 10.2172/5569909

Boiteau, R. M., and Repeta, D. J. (2015). An extended siderophore suite from synechococcus sp. PCC 7002 revealed by LC-ICPMS-ESIMS. *Metallomics* 7 (5), 877–884. doi: 10.1039/c5mt00005j

Bonnet, S., Guieu, C., Taillandier, V., Boulart, C., Bouruet-Aubertot, P., Gazeau, F., et al. (2023). Natural iron fertilization by shallow hydrothermal sources fuels diazotroph blooms in the ocean. *Science* 380, 812-817. doi: 10.1126/science.abq4654

Boye, M., Nishioka, J., Croot, P., Laan, P., Timmermans, K. R., Strass, V. H., et al. (2010). Significant portion of dissolved organic Fe complexes in fact is Fe colloids. *Mar. Chem.* 122 (1-4), 20–27. doi: 10.1016/j.marchem.2010.09.001

Buck, K. N., Lohan, M. C., Berger, C. J., and Bruland, K. W. (2007). Dissolved iron speciation in two distinct river plumes and an estuary: Implications for riverine iron supply. *Limnol. Oceanogr.* 52 (2), 843–855. doi: 10.4319/lo.2007.52.2.0843

Buck, K. N., Sedwick, P. N., Sohst, B., and Carlson, C. A. (2018). Organic complexation of iron in the eastern tropical South Pacific: results from US GEOTRACES Eastern Pacific Zonal Transect (GEOTRACES cruise GP16). *Mar. Chem.* 201, 229–241. doi: 10.1016/j.marchem.2017.11.007

Bundy, R. M., Abdulla, H. A., Hatcher, P. G., Biller, D. V., Buck, K. N., and Barbeau, K. A. (2015). Iron-binding ligands and humic substances in the San Francisco Bay estuary and estuarine-influenced shelf regions of coastal California. *Mar. Chem.* 173, 183–194. doi: 10.1016/j.marchem.2014.11.005

Bundy, R. M., Biller, D. V., Buck, K. N., Bruland, K. W., and Barbeau, K. A. (2014). Distinct pools of dissolved iron-binding ligands in the surface and benthic boundary layer of the California Current. *Limnol. Oceanogr.* 59 (3), 769–787. doi: 10.4319/lo.2014.59.3.0769

Bundy, R. M., Boiteau, R. M., McLean, C., Turk-Kubo, K. A., McIlvin, M. R., Saito, M. A., et al. (2018). Distinct siderophores contribute to iron cycling in the mesopelagic at station ALOHA. *Front. Mar. Sci.* 5. doi: 10.3389/fmars.2018.00061

Byrne, R. H., Luo, Y. R., and Young, R. W. (2000). Iron hydrolysis and solubility revisited: observations and comments on iron hydrolysis characterizations. *Mar. Chem.* 70 (1-3), 23–35. doi: 10.1016/S0304-4203(00)00012-8

Cabanes, D. J., Norman, L., Bowie, A. R., Strmečki, S., and Hassler, C. S. (2020). Electrochemical evaluation of iron-binding ligands along the Australian GEOTRACES southwestern Pacific section (GP13). *Mar. Chem.* 219, 103736. doi: 10.1016/j.marchem.2019.103736

Chen, M., and Wang, W. X. (2001). Bioavailability of natural colloid-bound iron to marine plankton: Influences of colloidal size and aging. *Limnol. Oceanogr.* 46 (8), 1956–1967. doi: 10.4319/lo.2001.46.8.1956

Coates, J. D., Cole, K. A., Chakraborty, R., O'Connor, S. M., and Achenbach, L. A. (2002). Diversity and ubiquity of bacteria capable of utilizing humic substances as electron donors for anaerobic respiration. *Appl. Environ. Microbiol.* 68 (5), 2445–2452. doi: 10.1128/AEM.68.5.2445-2452.2002

Cotte, L., Chavagnac, V., Pelleter, E., Laës-Huon, A., Cathalot, C., Dulaquais, G., et al. (2020). Metal partitioning after *in situ* filtration at deep-sea vents of the Lucky Strike hydrothermal field (EMSO-Azores, Mid-Atlantic Ridge, 37° N). *Deep Sea Res. Part I: Oceanogr. Res. Papers* 157, 103204. doi: 10.1016/j.dsr.2019.103204

Cottrell, M. T., and Kirchman, D. L. (2000). Natural assemblages of marine proteobacteria and members of the Cytophaga-Flavobacter cluster consuming low- and high-molecular-weight dissolved organic matter. *Appl. Environ. Microbiol.* 66 (4), 1692–1697. doi: 10.1128/AEM.66.4.1692-1697.2000

Croot, P. L., and Heller, M. I. (2012). The importance of kinetics and redox in the biogeochemical cycling of iron in the surface ocean. *Front. Microbiol.* 3. doi: 10.3389/fmicb.2012.00219

Davies, G., and Ghabbour, E. (2003). *Humic substances: Nature's most versatile materials* (New York, USA: Taylor & Francis). doi: 10.4324/9780203487600

De Paolis, F., and Kukkonen, J. (1997). Binding of organic pollutants to humic and fulvic acids: influence of pH and the structure of humic material. *Chemosphere* 34 (8), 1693–1704. doi: 10.1016/S0045-6535(97)00026-X

Dulaquais, G., Breitenstein, J., Waeles, M., Marsac, R., and Riso, R. (2018b). Measuring dissolved organic matter in estuarine and marine waters: size-exclusion chromatography with various detection methods. *Environ. Chem.* 15 (7), 436–449. doi: 10.1071/EN18108

Dulaquais, G., Waeles, M., Breitenstein, J., Knoery, J., and Riso, R. (2020). Links between size fractionation, chemical speciation of dissolved copper and chemical speciation of dissolved organic matter in the Loire estuary. *Environ. Chem.* 17 (5), 385–399. doi: 10.1071/EN19137

Dulaquais, G., Waeles, M., Gerringa, L. J., Middag, R., Rijkenberg, M. J., and Riso, R. (2018a). The biogeochemistry of electroactive humic substances and its connection to iron chemistry in the North East Atlantic and the Western Mediterranean Sea. *J. Geophys. Res.: Oceans* 123 (8), 5481–5499. doi: 10.1029/2018JC014211

Field, M. P., and Sherrell, R. M. (2000). Dissolved and particulate Fe in a hydrothermal plume at 9 45′ N, East Pacific Rise:: Slow Fe (II) oxidation kinetics in Pacific plumes. *Geochim. Cosmochim. Acta* 64 (4), 619–628. doi: 10.1016/S0016-7037(99)00333-6

Fitzsimmons, J. N., and Boyle, E. A. (2014). Both soluble and colloidal iron phases control dissolved iron variability in the tropical North Atlantic Ocean. *Geochim. Cosmochim. Acta* 125, 539–550. doi: 10.1016/j.gca.2013.10.032

Fitzsimmons, J. N., Bundy, R. M., Al-Subiai, S. N., Barbeau, K. A., and Boyle, E. A. (2015). The composition of dissolved iron in the dusty surface ocean: An exploration using size-fractionated iron-binding ligands. *Mar. Chem.* 173, 125–135. doi: 10.1016/j.marchem.2014.09.002

Fitzsimmons, J. N., John, S. G., Marsay, C. M., Hoffman, C. L., Nicholas, S. L., Toner, B. M., et al. (2017). Iron persistence in a distal hydrothermal plume supported by dissolved–particulate exchange. *Nat. Geosci.* 10 (3), 195–201. doi: 10.1038/ngeo2900

Fourrier, P., Dulaquais, G., Guigue, C., Giamarchi, P., Sarthou, G., Whitby, H., et al. (2022). Characterization of the vertical size distribution, composition and chemical properties of dissolved organic matter in the (ultra) oligotrophic Pacific Ocean through a multi-detection approach. *Mar. Chem.* 240, 104068. doi: 10.1016/j.marchem.2021.104068

Garnier, C., Pižeta, I., Mounier, S., Benaïm, J. Y., and Branica, M. (2004). Influence of the type of titration and of data treatment methods on metal complexing parameters determination of single and multi-ligand systems measured by stripping voltammetry. *Analytica Chimica Acta* 505 (2), 263–275. doi: 10.1016/j.aca.2003.10.066

Gerringa, L. J., Gledhill, M., Ardiningsih, I., Muntjewerf, N., and Laglera, L. M. (2021). Comparing CLE-AdCSV applications using SA and TAC to determine the fe-binding characteristics of model ligands in seawater. *Biogeosciences* 18 (19), 5265–5289. doi: 10.5194/bg-18-5265-2021

Gerringa, L. J., Rijkenberg, M. J., Thuróczy, C. E., and Maas, L. R. (2014). A critical look at the calculation of the binding characteristics and concentration of iron complexing ligands in seawater with suggested improvements. *Environ. Chem.* 11 (2), 114–136. doi: 10.1071/EN13072

Gledhill, M. (2001). Electrospray ionisation-mass spectrometry of hydroxamate siderophores. *Analyst* 126, 1359–1362. doi: 10.1039/B101268L

Gledhill, M., and Buck, K. N. (2012). The organic complexation of iron in the marine environment: a review. *Front. Microbiol.* 3. doi: 10.3389/fmicb.2012.00069

Gledhill, M., and Gerringa, L. J. A. (2017). The effect of metal concentration on the parameters derived from complexometric titrations of trace elements in seawater—a model study. *Front. Mar. Sci.* 4. doi: 10.3389/fmars.2017.00254

Gledhill, M., and van den Berg, C. M. (1994). Determination of complexation of iron (III) with natural organic complexing ligands in seawater using cathodic stripping voltammetry. *Mar. Chem.* 47 (1), 41–54. doi: 10.1016/0304-4203(94)90012-4

Gledhill, M., Zhu, K., Rusiecka, D., and Achterberg, E. P. (2022). Competitive interactions between microbial siderophores and humic-like binding sites in European shelf sea waters. *Front. Mar. Sci.* 9. doi: 10.3389/FMARS.2022.855009

González, A. G., Cadena-Aizaga, M. I., Sarthou, G., González-Dávila, M., and Santana-Casiano, J. M. (2019). Iron complexation by phenolic ligands in seawater. *Chem. Geol.* 511, 380–388. doi: 10.1016/j.chemgeo.2018.10.017

González-Santana, D., González-Dávila, M., Lohan, M. C., Artigue, L., Planquette, H., Sarthou, G., et al. (2021). Variability in iron (II) oxidation kinetics across diverse hydrothermal sites on the northern Mid Atlantic Ridge. *Geochim. Cosmochim. Acta* 297, 143–157. doi: 10.1016/j.gca.2021.01.013

González-Santana, D., Lough, A. J., Planquette, H., Sarthou, G., Tagliabue, A., and Lohan, M. C. (2023). The unaccounted dissolved iron (II) sink: Insights from dFe (II) concentrations in the deep Atlantic Ocean. *Sci. Total Environ.* 862, 161179. doi: 10.1016/j.scitotenv.2022.161179

Guo, L., Santschi, P. H., and Warnken, K. W. (1995). Dynamics of dissolved organic carbon (DOC) in oceanic environments. *Limnol. Oceanogr.* 40 (8), 1392–1403. doi: 10.4319/lo.1995.40.8.1392

Hassler, C. S., van den Berg, C. M., and Boyd, P. W. (2017). Toward a regional classification to provide a more inclusive examination of the ocean biogeochemistry of iron-binding ligands. *Front. Mar. Sci.* 4. doi: 10.3389/fmars.2017.00019

Hassler, C., Cabanes, D., Blanco-Ameijeiras, S., Sander, S. G., and Benner, R. (2019). Importance of refractory ligands and their photodegradation for iron oceanic inventories and cycling. *Mar. Freshw. Res.* 71 (3), 311–320. doi: 10.1071/MF19213

Hawco, N. J., Barone, B., Church, M. J., Babcock-Adams, L., Repeta, D. J., Wear, E. K., et al. (2021). Iron depletion in the deep chlorophyll maximum: mesoscale eddies as natural iron fertilization experiments. *Global Biogeochem. Cycles* 35 (12), e2021GB007112. doi: 10.1029/2021GB007112

Hawkes, J. A., Connelly, D. P., Gledhill, M., and Achterberg, E. P. (2013). The stabilisation and transportation of dissolved iron from high temperature hydrothermal vent systems. *Earth Planet. Sci. Lett.* 375, 280–290. doi: 10.1016/j.epsl.2013.05.047

Hedges, J. I., Hatcher, P. G., Ertel, J. R., and Meyers-Schulte, K. J. (1992). A comparison of dissolved humic substances from seawater with Amazon River counterparts by 13C-NMR spectrometry. *Geochim. Cosmochim. Acta* 56 (4), 1753–1757. doi: 10.1016/0016-7037(92)90241-A

Hertkorn, N., Benner, R., Frommberger, M., Schmitt-Kopplin, P., Witt, M., Kaiser, K., et al. (2006). Characterization of a major refractory component of marine dissolved organic matter. *Geochim. Cosmochim. Acta* 70 (12), 2990–3010. doi: 10.1016/j.gca.2006.03.021

Hoffman, C. L., Schladweiler, C. S., Seaton, N. C., Nicholas, S. L., Fitzsimmons, J. N., Sherrell, R. M., et al. (2020). Diagnostic morphology and solid-state chemical speciation of hydrothermally derived particulate Fe in a long-range dispersing plume. *ACS Earth Space Chem.* 4 (10), 1831–1842. doi: 10.1021/acsearthspacechem.0c00067

Hunter, K. A., and Boyd, P. W. (2007). Iron-binding ligands and their role in the ocean biogeochemistry of iron. *Environ. Chem.* 4 (4), 221–232. doi: 10.1071/EN07012

Krachler, R., Krachler, R. F., Wallner, G., Hann, S., Laux, M., Recalde, M. F. C., et al. (2015). River-derived humic substances as iron chelators in seawater. *Mar. Chem.* 174, 85–93. doi: 10.1016/j.marchem.2015.05.009

Kuma, K., Nishioka, J., and Matsunaga, K. (1996). Controls on iron (III) hydroxide solubility in seawater: the influence of pH and natural organic chelators. *Limnol. Oceanogr.* 41 (3), 396–407. doi: 10.4319/lo.1996.41.3.0396

Kunde, K., Wyatt, N. J., González-Santana, D., Tagliabue, A., Mahaffey, C., and Lohan, M. C. (2019). Iron distribution in the subtropical North Atlantic: The pivotal role of colloidal iron. *Global Biogeochem. Cycles* 33 (12), 1532–1547. doi: 10.1029/2019GB006326

Laglera, L. M., Battaglia, G., and van den Berg, C. M. (2007). Determination of humic substances in natural waters by cathodic stripping voltammetry of their complexes with iron. *Anal. Chim. Acta* 599 (1), 58–66. doi: 10.1016/j.aca.2007.07.059

Laglera, L. M., Battaglia, G., and van den Berg, C. M. (2011). Effect of humic substances on the iron speciation in natural waters by CLE/CSV. *Mar. Chem.* 127 (1-4), 134–143. doi: 10.1016/j.marchem.2011.09.003

Laglera, L. M., Sukekava, C., Slagter, H. A., Downes, J., Aparicio-Gonzalez, A., and Gerringa, L. J. (2019). First quantification of the controlling role of humic substances in the transport of iron across the surface of the Arctic Ocean. *Environ. Sci. Technol.* 53 (22), 13136–13145. doi: 10.1021/acs.est.9b04240

Laglera, L. M., and van den Berg, C. M. (2009). Evidence for geochemical control of iron by humic substances in seawater. *Limnol. Oceanogr.* 54 (2), 610–619. doi: 10.4319/lo.2009.54.2.0610

Liu, X., and Millero, F. J. (2002). The solubility of iron in seawater. *Mar. Chem.* 77 (1), 43–54. doi: 10.1016/S0304-4203(01)00074-3

Lough, A. J. M., Homoky, W. B., Connelly, D. P., Comer-Warner, S. A., Nakamura, K., Abyaneh, M. K., et al. (2019). Soluble iron conservation and colloidal iron dynamics in a hydrothermal plume. *Chem. Geol.* 511, 225–237. doi: 10.1016/j.chemgeo.2019.01.001

Lough, A. J., Tagliabue, A., Demasy, C., Resing, J. A., Mellett, T., Wyatt, N. J., et al. (2023). Tracing differences in iron supply to the Mid-Atlantic Ridge valley between hydrothermal vent sites: implications for the addition of iron to the deep ocean. *Biogeosciences* 20 (2), 405–420. doi: 10.5194/bg-20-405-2023

MacCarthy, P., Peterson, M. J., Malcolm, R. L., and Thurman, E. M. (1979). Separation of humic substances by pH gradient desorption from a hydrophobic resin. *Anal. Chem.* 51 (12), 2041–2043. doi: 10.1021/ac50048a036

Macrellis, H. M., Trick, C. G., Rue, E. L., Smith, G., and Bruland, K. W. (2001). Collection and detection of natural iron-binding ligands from seawater. *Mar. Chem.* 76 (3), 175–187. doi: 10.1016/S0304-4203(01)00061-5

Maillard, L. C. (1912). Action des acides aminés sur les sucres; formation des mélanoïdines par voie méthodique. *CR Acad. Sci. Paris* 154, 66–68. Available at: https://gallica.bnf.fr/ark:/12148/bpt6k31070/f72.tableDesMatieres.

Martin, J. H., and Fitzwater, S. E. (1988). Iron deficiency limits phytoplankton growth in the north-east Pacific subarctic. *Nature* 331 (6154), 341–343. doi: 10.1038/331341a0

Martin, J. H., and Gordon, R. M. (1988). Northeast Pacific iron distributions in relation to phytoplankton productivity. *Deep Sea Res. Part A. Oceanogr. Res. Papers* 35 (2), 177–196. doi: 10.1016/0198-0149(88)90035-0

Martin, J. H., Gordon, M., and Fitzwater, S. E. (1991). The case for iron. *Limnol. Oceanogr.* 36 (8), 1793–1802. doi: 10.4319/lo.1991.36.8.1793

Martin, J. H., Gordon, R. M., Fitzwater, S., and Broenkow, W. W. (1989). Vertex: phytoplankton/iron studies in the Gulf of Alaska. *Deep Sea Res. Part A. Oceanogr. Res. Papers* 36 (5), 649–680. doi: 10.1016/0198-0149(89)90144-1

Mawji, E., Gledhill, M., Milton, J. A., Tarran, G. A., Ussher, S., Thompson, A., et al. (2008). Hydroxamate siderophores: Occurrence and importance in the Atlantic Ocean. *Environ. Sci. Technol.* 42, 8675–8680. doi: 10.1021/es801884r

McCormack, P., Worsfold, P. J., and Gledhill, M. (2003). Separation and detection of siderophores produced by marine bacterioplankton using high-performance liquid chromatography with electrospray ionization mass spectrometry. *Anal. Chem.* 75, 2647–2652. doi: 10.1021/ac0340105

Millero, F. J., Sotolongo, S., and Izaguirre, M. (1987). The oxidation kinetics of Fe (II) in seawater. *Geochim. Cosmochim. Acta* 51 (4), 793–801. doi: 10.1016/0016-7037(87)90093-7

Misumi, K., Lindsay, K., Moore, J. K., Doney, S. C., Tsumune, D., and Yoshida, Y. (2013). Humic substances may control dissolved iron distributions in the global ocean: Implications from numerical simulations. *Global Biogeochem. Cycles* 27 (2), 450–462. doi: 10.1002/gbc.20039

Moore, C. M., Mills, M. M., Arrigo, K. R., Berman-Frank, I., Bopp, L., Boyd, P. W., et al. (2013). Processes and patterns of oceanic nutrient limitation. *Nat. Geosci.* 6 (9), 701–710. doi: 10.1038/ngeo1765

Nishioka, J., Takeda, S., Wong, C. S., and Johnson, W. K. (2001). Size-fractionated iron concentrations in the northeast Pacific Ocean: distribution of soluble and small colloidal iron. *Mar. Chem.* 74 (2-3), 157–179. doi: 10.1016/S0304-4203(01)00013-5

Obernosterer, I., Reitner, B., and Herndl, G. J. (1999). Contrasting effects of solar radiation on dissolved organic matter and its bioavailability to marine bacterioplankton. *Limnol. Oceanogr.* 44 (7), 1645–1654. doi: 10.4319/lo.1999.44.7.1645

Perdue, E. M., and Lytle, C. R. (1983). A distribution model for binding of protons and metal ions by humic substances. *Environ. Sci. Technol.* 17 (11), 654–660. doi: 10.1021/es00117a006

Pérez-Almeida, N., González, A. G., Santana-Casiano, J. M., and González-Dávila, M. (2022). Ocean acidification effect on the iron-gallic acid redox interaction in seawater. *Front. Mar. Sci.* 9. doi: 10.3389/fmars.2022.837363

Pižeta, I., Sander, S. G., Hudson, R. J. M., Omanović, D., Baars, O., Barbeau, K. A., et al. (2015). Interpretation of complexometric titration data: An intercomparison of methods for estimating models of trace metal complexation by natural organic ligands. *Mar. Chem.* 173, 3–24. doi: 10.1016/j.marchem.2015.03.006

Plank, S., Marchese, F., Genzano, N., Nolde, M., and Martinis, S. (2020). The short life of the volcanic island New Late'iki (Tonga) analyzed by multi-sensor remote sensing data. *Sci. Rep.* 10 (1), 1–15. doi: 10.1038/s41598-020-79261-7

Resing, J. A., Sedwick, P. N., German, C. R., Jenkins, W. J., Moffett, J. W., Sohst, B. M., et al. (2015). Basin-scale transport of hydrothermal dissolved metals across the South Pacific Ocean. *Nature* 523 (7559), 200–203. doi: 10.1038/nature14577

Rich, H. W., and Morel, F. M. (1990). Availability of well-defined iron colloids to the marine diatom Thalassiosira weissflogii. *Limnol. Oceanogr.* 35 (3), 652–662. doi: 10.4319/lo.1990.35.3.0652

Riso, R., Mastin, M., Aschehoug, A., Davy, R., Devesa, J., Laës-Huon, A., et al. (2021). Distribution, speciation and composition of humic substances in a macro-tidal temperate estuary. *Estuarine Coast. Shelf Sci.* 255, 107360. doi: 10.1016/j.ecss.2021.107360

Rose, A. L., and Waite, T. D. (2003a). Kinetics of iron complexation by dissolved natural organic matter in coastal waters. *Mar. Chem.* 84 (1-2), 85–103. doi: 10.1016/S0304-4203(03)00113-0

Rose, A. L., and Waite, T. D. (2003b). Kinetics of hydrolysis and precipitation of ferric iron in seawater. *Environ. Sci. Technol.* 37 (17), 3897–3903. doi: 10.1021/es034102b

Rosenstock, B., Zwisler, W., and Simon, M. (2005). Bacterial consumption of humic and non-humic low and high molecular weight DOM and the effect of solar irradiation on the turnover of labile DOM in the Southern Ocean. *Microb. Ecol.* 50 (1), 90–101. doi: 10.1007/s00248-004-0116-5

Ruacho, A., Bundy, R. M., Till, C. P., Roshan, S., Wu, J., and Barbeau, K. A. (2020). Organic dissolved copper speciation across the US GEOTRACES equatorial Pacific zonal transect GP16. *Mar. Chem.* 225, 103841. doi: 10.1016/j.marchem.2020.103841

Rue, E. L., and Bruland, K. W. (1995). Complexation of iron (III) by natural organic ligands in the Central North Pacific as determined by a new competitive ligand equilibration/adsorptive cathodic stripping voltammetric method. *Mar. Chem.* 50 (1-4), 117–138. doi: 10.1016/0304-4203(95)00031-L

Sander, S. G., and Koschinsky, A. (2011). Metal flux from hydrothermal vents increased by organic complexation. *Nat. Geosci.* 4 (3), 145–150. doi: 10.1038/ngeo1088

Santana-Casiano, J. M., González-Dávila, M., and Millero, F. J. (2005). Oxidation of nanomolar levels of Fe (II) with oxygen in natural waters. *Environ. Sci. Technol.* 39 (7), 2073–2079. doi: 10.1021/es049748y

Santana-Casiano, J. M., González-Santana, D., Devresse, Q., Hepach, H., Santana-González, C., Quack, B., et al. (2022). Exploring the effects of organic matter characteristics on Fe (II) oxidation kinetics in coastal seawater. *Environ. Sci. Technol.* 56 (4), 2718–2728. doi: 10.1021/acs.est.1c04512

Schlitzer, R., Anderson, R. F., Dodas, E. M., Lohan, M., Geibert, W., Tagliabue, A., et al. (2018). The GEOTRACES intermediate data product 2017. *Chem. Geol.* 493, 210–223. doi: 10.1016/j.chemgeo.2018.05.040

Schlitzer, R. (2022) *Ocean data view*. Available at: https://odv.awi.de/.

Shaw, T. J., Luther, G. W.III, Rosas, R., Oldham, V. E., Coffey, N. R., Dias, D. M. C., et al. (2021). Fe-catalyzed sulfide oxidation in hydrothermal plumes is a source of reactive oxygen species to the ocean. *PNAS* 118 (40). doi: 10.1073/pnas.2026654118

Slagter, H. A., Laglera, L. M., Sukekava, C., and Gerringa, L. J. (2019). Fe-binding organic ligands in the humic-rich TransPolar Drift in the surface Arctic Ocean using multiple voltammetric methods. *J. Geophys. Res.: Oceans* 124 (3), 1491–1508. doi: 10.1029/2018JC014576

Slagter, H. A., Reader, H. E., Rijkenberg, M. J. A., van der Loeff, M. R., De Baar, H. J. W., and Gerringa, L. J. A. (2017). Organic Fe speciation in the Eurasian Basins of the Arctic Ocean and its relation to terrestrial DOM. *Mar. Chem.* 197, 11–25. doi: 10.1016/j.marchem.2017.10.005

Stedmon, C. A., and Cory, R. M. (2014). Biological origins and fate of fluorescent dissolved organic matter in aquatic environments. *Aquat. Organic Matter Fluorescence*, 278–299. doi: 10.1017/CBO9781139045452.013

Sukekava, C., Downes, J., Slagter, H. A., Gerringa, L. J., and Laglera, L. M. (2018). Determination of the contribution of humic substances to iron complexation in seawater by catalytic cathodic stripping voltammetry. *Talanta* 189, 359–364. doi: 10.1016/j.talanta.2018.07.021

Sung, W., and Morgan, J. J. (1980). Kinetics and product of ferrous iron oxygenation in aqueous systems. *Environ. Sci. Technol.* 14 (5), 561–568. doi: 10.1021/es60165a006

Tagliabue, A., Bopp, L., Dutay, J. C., Bowie, A. R., Chever, F., Jean-Baptiste, P., et al. (2010). Hydrothermal contribution to the oceanic dissolved iron inventory. *Nat. Geosci.* 3 (4), 252–256. doi: 10.1038/ngeo818

Tagliabue, A., Lough, A. J., Vic, C., Roussenov, V., Gula, J., Lohan, M. C., et al. (2022). Mechanisms driving the dispersal of hydrothermal iron from the northern Mid Atlantic Ridge. *Geophys. Res. Lett.* 49 (22), e2022GL100615. doi: 10.1029/2022GL100615

Tani, H., Nishioka, J., Kuma, K., Takata, H., Yamashita, Y., Tanoue, E., et al. (2003). Iron (III) hydroxide solubility and humic-type fluorescent organic matter in the deep water column of the Okhotsk Sea and the northwestern North Pacific Ocean. *Deep Sea Res. Part I: Oceanogr. Res. Papers* 50 (9), 1063–1078. doi: 10.1016/S0967-0637(03)00098-0

Thurman, E. M., and Malcolm, R. L. (1981). Preparative isolation of aquatic humic substances. *Environ. Sci. Technol.* 15 (4), 463–466. doi: 10.1021/es00086a012

Tilliette, C., Taillandier, V., Bouruet-Aubertot, P., Grima, N., Maes, C., Montanes, M., et al. (2022). Dissolved iron patterns impacted by shallow hydrothermal sources along a transect through the Tonga-Kermadec arc. *Global Biogeochemical Cycle* 36 (7), e2022GB007363. doi: 10.1029/2022GB007363

Town, R. M., and Filella, M. (2000). Dispelling the myths: Is the existence of L1 and L2 ligands necessary to explain metal ion speciation in natural waters? *Limnol. Oceanogr.* 45 (6), 1341–1357. doi: 10.4319/lo.2000.45.6.1341

Tranvik, L. J. (1993). Microbial transformation of labile dissolved organic matter into humic-like matter in seawater. *FEMS Microbiol. Ecol.* 12 (3), 177–183. doi: 10.1111/j.1574-6941.1993.tb00030.x

van den Berg, C. M. (1995). Evidence for organic complexation of iron in seawater. *Mar. Chem.* 50 (1-4), 139–157. doi: 10.1016/0304-4203(95)00032-M

Von der Heyden, B. P., Roychoudhury, A. N., Mtshali, T. N., Tyliszczak, T., and Myneni, S. C. B. (2012). Chemically and geographically distinct solid-phase iron pools in the Southern Ocean. *Science* 338 (6111), 1199–1201. doi: 10.1126/science.1227504

Waeles, M., Cotte, L., Pernet-Coudrier, B., Chavagnac, V., Cathalot, C., Leleu, T., et al. (2017). On the early fate of hydrothermal iron at deep-sea vents: A reassessment after *in situ* filtration. *Geophysical Res. Lett.* 44 (9), 4233–4240. doi: 10.1002/2017GL073315

Wang, W. X., and Dei, R. C. (2003). Bioavailability of iron complexed with organic colloids to the cyanobacteria Synechococcus and Trichodesmium. *Aquat. Microb. Ecol.* 33 (3), 247–259. doi: 10.3354/ame033247

Wang, H., Resing, J. A., Yan, Q., Buck, N. J., Michael, S. M., Zhou, H., et al. (2021). The characteristics of Fe speciation and Fe-binding ligands in the Mariana back-arc hydrothermal plumes. *Geochim. Cosmochim. Acta* 292, 24–36. doi: 10.1016/j.gca.2020.09.016

Wang, H., Wang, W., Liu, M., Zhou, H., Ellwood, M. J., Butterfield, D. A., et al. (2022). Iron ligands and isotopes in hydrothermal plumes over backarc volcanoes in the Northeast Lau Basin, Southwest Pacific Ocean. *Geochim. Cosmochim. Acta* 336, 341–352. doi: 10.1016/j.gca.2022.09.026

Whitby, H., Bressac, M., Sarthou, G., Ellwood, M. J., Guieu, C., and Boyd, P. W. (2020a). Contribution of electroactive humic substances to the iron-binding ligands released during microbial remineralization of sinking particles. *Geophys. Res. Lett.* 47 (7). doi: 10.1029/2019GL086685

Whitby, H., Planquette, H., Cassar, N., Bucciarelli, E., Osburn, C. L., Janssen, D. J., et al. (2020b). A call for refining the role of humic-like substances in the oceanic iron cycle. *Sci. Rep.* 10 (1), 1–12. doi: 10.1038/s41598-020-62266-7

Whitby, H., and van den Berg, C. M. (2015). Evidence for copper-binding humic substances in seawater. *Mar. Chem.* 173, 282–290. doi: 10.1016/j.marchem.2014.09.011

Wu, J., Boyle, E., Sunda, W., and Wen, L. S. (2001). Soluble and colloidal iron in the oligotrophic North Atlantic and North Pacific. *Science* 293 (5531), 847–849. doi: 10.1126/science.1059251

Wu, J., and Luther, G. W.III (1995). Complexation of Fe (III) by natural organic ligands in the Northwest Atlantic Ocean by a competitive ligand equilibration method and a kinetic approach. *Mar. Chem.* 50 (1-4), 159–177. doi: 10.1016/0304-4203(95)00033-N

Ye, Y., Völker, C., and Gledhill, M. (2020). Exploring the iron-binding potential of the ocean using a combined pH and DOC parameterization. *Global Biogeochem. Cycles* 34 (6), e2019GB006425. doi: 10.1029/2019GB006425

Zhu, K., Birchill, A. J., Milne, A., Ussher, S., Humphreys, M. P., Carr, N., et al. (2021). Equilibrium calculations of iron speciation and apparent iron solubility in the Celtic Sea at ambient seawater pH using the NICA-Donnan model. *Mar. Chem.* 237, 104038. doi: 10.1016/j.marchem.2021.104038

Zigah, P. K., McNichol, A. P., Xu, L., Johnson, C., Santinelli, C., Karl, D. M., et al. (2017). Allochthonous sources and dynamic cycling of ocean dissolved organic carbon revealed by carbon isotopes. *Geophys. Res. Lett.* 44 (5), 2407–2415. doi: 10.1002/2016GL071348